Noncontact orientation of objects in three-dimensional space using magnetic levitation

Non-Contact Orientation of Objects in Three Dimensional Space Using Magnetic Levitation

Anand Bala Subramaniam,[a] Dian Yang,[b] Hai-Dong Yu,[a] Alex Nemiroski,[a] Simon Tricard,[a] Audrey K. Ellerbee,[a] Siowling Soh[a], and George M. Whitesides [a,c,d]*

[a] Department of Chemistry & Chemical Biology, Harvard University, Cambridge, MA 02138
[b] School of Engineering and Applied Science, Harvard University, Cambridge, MA 02138
[c] Wyss Institute for Biologically Inspired Engineering, Harvard University, Cambridge, MA 02138 USA
[d] The Kavli Institute for Bionano Science, Harvard University, Cambridge, MA 02138 USA

Corresponding author:
George M. Whitesides
230 Mallinkrodt Bldg.
Harvard University
12 Oxford St.
Cambridge, MA 02138
(617) 495-9430
gwhitesides@gmwgroup.harvard.edu

Classification:
Physical Sciences: (1) Applied Physical Sciences (2) Chemistry

Keywords:

Magnetic Levitation, Orientation, Soft Materials, Transitions, Manufacturing, Robotics, Self-Assembly

SIGNIFICANCE STATEMENT

We describe several non-contact methods of orienting objects in three-dimensional (3D) space using Magnetic Levitation (MagLev), and report the discovery of a sharp geometry-dependent transition of the orientation of levitating objects. An analytical theory of the orientation of arbitrary objects in Maglev explains this transition. MagLev is capable of manipulating and orienting hard and soft objects, and objects of irregular shape. Since controlling the orientation of objects in space is a prerequisite for assembling complex structures from simpler components, this paper extends magnetic levitation into 3D self-assembly, robotic assembly, and non-contact (stiction-free) orientation of hard and soft objects for applications in biomimetics, soft robotics, and stimulus responsive materials, among others.

Abstract

This paper describes several non-contact methods of orienting objects in three-dimensional (3D) space using Magnetic Levitation (MagLev). The methods use two permanent magnets arranged coaxially with like-poles facing (an anti-Helmholtz configuration) and a container containing a paramagnetic liquid in which the objects are suspended. Absent external forcing, objects levitating in the device adopt predictable static orientations; the orientation depends on the shape and distribution of mass within the objects. The orientation of objects of uniform density in the MagLev device shows a sharp geometry-dependent transition: an analytical theory rationalizes this transition and predicts the orientation of objects in the MagLev device. Manipulation of the orientation of the levitating objects *in space* is achieved in two ways: i) by rotating and/or translating the MagLev device while the objects are suspended in the paramagnetic solution between the magnets; ii) by moving a small external magnet close to the levitating objects while keeping the device stationary. Unlike mechanical agitation or robotic selection, orienting using MagLev is possible for objects having a range of different physical characteristics (e.g., different shapes, sizes, and mechanical properties from hard polymers to gels and fluids). Magnetic levitation thus has the potential to be useful for sorting and positioning components in 3D space, orienting objects for assembly, constructing non-contact devices, and assembling objects composed of soft materials such as hydrogels, elastomers, and jammed granular media.

\body

Introduction

Developing new techniques to manipulate and orient components is part of the developing field of advanced manufacturing. Procedures for orienting hard objects reliably in three dimensions (3D) are essential for many existing manufacturing processes and relevant to a range of applications in other areas (1). Examples include operating automated manufacturing lines, sorting and pre-positioning components for assembly, and inspecting parts for quality control. Components in assembly lines often have random orientations, and they must be oriented properly before assembly (2-4). Advanced and 'next-generation' approaches based on biomimetic (5-8) and soft robotic (9) strageties, and hierarchically organized, self-assembled, and stimulus-responsive materials (10-15) particularly require methods capable of orienting and assembling soft, sticky, and easily damaged materials. Few methods exist to manipulate these types of materials without damaging them.

One way of orienting hard objects is to agitate them mechanically, and to allow them to fit (or fall) into openings of complementary shape (2); for appropriate geometries, a correct fit ensures that the object is appropriately oriented and can be transported to the next process. The disadvantages of this method are that it can be slow, and that it is not suitable for objects that are soft, fragile, or sticky. Most importantly, it is only reliable for objects of anisotropic shape: that is, it fails for objects that have only slightly asymmetrical shapes or sizes (16, 17).

Robotics provides an alternative method for orienting hard objects. Robotic arms can grasp and arbitrarily position objects that are randomly oriented, but to do so, they require imaging devices, sensors and complex control algorithms (3). Such robots, therefore, must incorporate complex, expensive vision systems (18); such systems also do not work well with soft materials

(19, 20) (although soft robots (21, 22) and grippers (23) may develop to a level at which they ease the task of manipulating soft or fragile objects). In general, automated systems (e.g., "pick-and-place" robotic systems) handle objects of specific shapes, and are not designed for general-purpose recognition and manipulation of objects of arbitrary shapes and materials (24, 25). Thus, changes in a manufacturing process may require extensive modifications to a robotic system before it can handle objects of (even slightly) different shapes or sizes (26).

This paper describes several non-contact methods of orienting both hard and soft objects of different shapes and sizes using Magnetic Levitation (MagLev). Objects are suspended in aqueous solutions of a paramagnetic salt (e.g., $MnCl_2$), and levitated against gravity in a magnetic field gradient generated by two NdFeB magnets arranged with like poles facing each other (a MagLev device, see Fig. 1) (27, 28). Historically, magnetic levitation, in air, of strongly diamagnetic materials (29) such as bismuth and pyrolytic graphite has been used to create devices such as a frictionless rotor (30), a tiltmeter/seismometer (31) and a pressure gauge (32). We and others have used magnetic levitation in paramagnetic liquids for trapping small objects and separating diamagnetic materials on the basis of differences in density (28, 29, 33-47). This paper extends MagLev to the manipulation and orientation of objects of uniform density in 3D space. Non-spherical objects levitate with a well-defined orientation in the device. When the density of the object is uniform, the orientation that the levitating object adopts in the device depends only on the shape and aspect ratio of the object. We discovered a sharp, aspect ratio-dependent transition in the orientation of objects levitating in the MagLev device. We present an analytical theory that explains this transition, and predicts the orientation of objects in the MagLev device.

The orientation of levitating objects in space can be manipulated in two ways: i) by rotating and/or translating the MagLev device (with the objects suspended between the magnets), ii) by

keeping the MagLev device stationary while perturbing the magnetic field externally (e.g., by moving a small magnet or ferromagnetic probe close to the levitating objects).

Background. The MagLev device that we used was similar to the ones previously described (27, 47). Finite element simulations based on the parameters (dimensions, strength of the magnetic field, magnetic susceptibility of the solution) of this device show that, to a good approximation, the gradient of the magnetic field is linear, with a constant slope between the surface of the top magnet to the surface of the bottom magnet, and the magnetic field is zero at the center of the device (27).

When an object is immersed in a (paramagnetic) liquid, it experiences a gravitational force, $\vec{F}_g$, due to the difference in densities between the object, ρ_o (kg m^{-3}), and the solution, ρ_s (kg m^{-3}) (Fig. 1). In Equation (1), V (m^3) is the volume of the object and g (m s^{-2}) is the acceleration due to gravity. By convention, we take the direction towards the center of the earth as positive. The gravitational force, $\vec{F}_g$, acts upwards when the object has a lower density than the liquid, downwards when the object has a higher density than the liquid, and is zero when the object has the same density as the liquid.

$$\vec{F}_g = (\rho_o - \rho_s)V\vec{g} \qquad (1)$$

When placed in the MagLev device, an object with a magnetic susceptibility χ_o (χ_o is dimensionless and is typically on the order of 10^{-5} for diamagnetic objects (27)), that is different from the magnetic susceptibility of the paramagnetic solution, χ_s ($\chi_s \sim 1.8 \times 10^{-4}$ for 1.00 M $MnCl_2$ (27)), experiences a magnetic force, $\vec{F}_{mag}$, given by Equation (2) (27). In Eq. 2, $\vec{B}$ is the

applied magnetic field (T) and $\mu_0 = 4\,\pi \times 10^{-2}$ (N A^{-2}) is the magnetic permeability of free space.

$$\vec{F}_{mag} = \frac{(\chi_o - \chi_s)}{\mu_o} V\, \vec{B} \cdot \left(\nabla \vec{B}\right) \qquad (2)$$

The magnetic force arises due to the interaction between the paramagnetic liquid and the gradient in the magnetic field between the two coaxial magnets. In a gradient of magnetic field, maximizing the volume of paramagnetic liquid in regions of high magnetic field strength minimizes the potential energy of the system. Thus, in a MagLev device, the magnetic force acts to displace diamagnetic objects towards the center of the device, where the magnitude of the field is lowest. This movement of diamagnetic objects away from high-field regions allows the volume of paramagnetic liquid displaced by the object to occupy regions of higher relative field strength closer to the surface of the magnets.

An object levitates stably when the gravitational and magnetic forces balance. Equation (3) gives the levitation height *h* (Fig.1) at which this equilibrium is achieved for a point-like object (27). In this equation, *d* (m) is the separation distance between the magnets, and B_o is the magnitude of the magnetic field at the surface of the magnets. To a good approximation, Eq. 3 also describes the levitation height of the center of volume of finite-sized, homogenous spherical objects (and less generally of objects that are heterogeneous and/or non-spherical) in the MagLev device (27, 47).

$$h = \frac{(\rho_o - \rho_s) g \mu_o d^2}{(\chi_o - \chi_s) 4 {B_o}^2} + \frac{d}{2} \qquad (3)$$

If $\vec{F}_g > \vec{F}_{mag}$ everywhere in the device, the objects sinks, and if $\vec{F}_g < \vec{F}_{mag}$ everywhere in the device, the object rises. Thus, only values of h from 0 to the height of the meniscus of the paramagnetic liquid are relevant practically, although Eq. 3 can, in principle, provide values of h ranging from $-\infty$ to $+\infty$.

Convention for Describing Orientation. Non-spherical objects adopt distinguishable orientations in the MagLev device (and, by extension, a fixed laboratory frame of reference). Here we describe the convention we adopt to describe our results. We use Cartesian coordinates. The fixed coordinates (i.e., the laboratory frame of reference) are the *x*-, *y*-, and *z*- axes. The MagLev device may be rotated relative to the laboratory frame of reference, and thus we define a body-fixed coordinate system, *x'*-, *y'*-, *z'*-, for the device (Fig. 1). To describe the orientation of objects with obvious (even if approximate) axes of symmetry (e.g., the long axis of a screw or a cylinder), we define a normalized direction vector $\vec{p}$ (Fig. 1 inset). The direction of $\vec{p}$ could, in principle, be chosen arbitrarily, but for objects with obvious axes of symmetry, it is usually convenient to define $\vec{p}$ to be aligned with one such axis.

Results and Discussion

The Orientations of Non-spherical Objects Levitating in a MagLev Device. As a preliminary study, we levitated a Nylon screw (9 mm in length) in the MagLev device. In these experiments, we rested the MagLev device on a flat laboratory bench, and hence the *x'*-, *y'*-, *z'*- axes coincided with the *x*-, *y*-, *z*- axes of the laboratory frame of reference. The concentration of $MnCl_2$ was

1.50 M, yielding a solution of density ρ_s ~ 1.15 g/cm³ (measured with a pycnometer). The density of the solution was similar to that of the screw, ρ_o = 1.15 g/cm³ (manufacturer's data). We chose the direction vector $\vec{p}$ to point along the long axis of the screw. The screw levitated at the center of the device and adopted an orientation with $\vec{p}$ parallel to the surface of the magnets (Fig. 2A). We next modified the shape of the screw by cutting the shaft to a length of 2.5 mm. The shortened screw, while still levitating at the center of the device, adopted an orientation with $\vec{p}$ pointing perpendicular to the surface of the magnets (Fig. 2B). Since we only changed the geometry of the screw, albeit substantially, we inferred that geometry played a role in determining the orientation of objects in this MagLev device.

We designed a series of experiments with model objects to explore the role of geometry for orientation in the MagLev device. We machined objects out of organic polymers with circular, annular, square, and triangular two-dimensional cross sections, each with a constant 'characteristic' length, ℓ. Depending on the object, ℓ was the diameter of the circle, the outer diameter of the annulus, the side width of the square, or the length of the sides of the equilateral triangle (Fig. 2C-F). We varied the thickness, T, of the objects in the third dimension to produce cylinders, annular cylinders, square prisms, and triangular prisms. Levitating these relatively simple, symmetric 3D objects with MagLev allowed us to obtain a theoretical understanding of the governing physics. To classify the shapes, we defined a non-dimensional aspect ratio parameter, A_R, to be the ratio between the thickness of the object and its characteristic length (i.e., $A_R = T/\ell$; see Fig. 2). We set $\vec{p}$ to be aligned along the thickness axis of the object.

We started by levitating objects of small A_R, and progressively levitated objects with larger A_R. We captured images of the objects along the y'-z' plane and measured the angle α that $\vec{p}$ subtended with respect to the z'- axis of the device. We defined α to be zero when $\vec{p}$ was parallel to the z'-axis. The value of α was clustered either around 0° or 90° — $\vec{p}$ was parallel or

perpendicular to the surface of the magnets — with at most a 10° (typically < 5°) variation observed between replicate objects. Plots of α versus A_R for each of the shapes revealed that α jumped abruptly from 0° to 90° at what appeared to be a critical value of A_R, which we denote as A_R^*. The value of A_R^* appeared to be different for the different shapes. For the cylinder we observed $0.84 \leq A_R^* \leq 0.88$, for the annular cylinder we observed $1.04 \leq A_R^* \leq 1.12$, for the square prism we observed $0.90 \leq A_R^* \leq 1.10$, and for the triangular prism we observed $0.65 \leq A_R^* \leq 0.73$. The value of A_R^* and the orientation of the objects in the *y'-z'* plane did not depend on the shape of the magnets, the levitation height of the objects (Fig. S1) and the distance, *d*, between the two magnets (varied from 45 mm to 65 mm) (Fig. S2), suggesting that the observed effects are purely a function of the shape of the objects.

The orientation of the object in the *x'-y'* plane, as expected, did depend on the shape of the magnets. For square magnets, the objects centered in the magnetic field and aligned along the diagonals (Fig. S3). For disc-shaped magnets, the final orientation of the object in the *x'-y'* plane was dependent on the history of sample. Shaking the container, or removing the container and replacing it in the MagLev device, caused the orientation of the object in this plane to change (data not shown). The orientation of the object in the *y'-z'* plane, however, was still fixed and determined only by A_R.

Modeling the Height and Orientation of Non-spherical Objects in MagLev. The dependence of the height and orientation of objects on shape was one for which we wished to have an analytical treatment. Rather than work with equations of force (Eq. 1, Eq. 2), which, without modification, are valid strictly for point-like objects, we consider the potential energy of an arbitrary object located in a region with superimposed magnetic and gravitational fields (a

MagLev system). Equation (4) gives the energy density (energy per unit volume) of the MagLev system.

$$u = u_{mag} + u_{grav} = -\frac{1}{2\mu_o}\Delta\chi(\vec{r})\vec{B}^2 - \Delta\rho(\vec{r})\vec{g}\cdot\vec{h}, \quad (4)$$

In this equation, u_{mag} is the magnetic contribution and u_{grav} is the gravitational contribution to the total potential energy density, $\Delta\chi(\vec{r}) = \chi_o(\vec{r}) - \chi_s$ is the magnetic susceptibility of the object relative to a homogenous medium, $\Delta\rho(\vec{r}) = \rho_o(\vec{r}) - \rho_s$ is the density of the object relative to a homogenous medium, and $\vec{h} = (0,0,h)$ is the height of the object. In general, the object can be heterogeneous in both density and magnetic susceptibility such that these functions depend on the position coordinate $\vec{r}$. Note that taking the negative of the derivative of u_{grav} and u_{mag} with respect to *z'* gives Eq. 1 and Eq. 2, as expected.

At static equilibrium, the potential energy, $U = \int_V u\, dV$, where *V* is the volume of the object, has to be minimized. Finding the equilibrium configuration involves minimizing simultaneously the energy associated with the levitation height and orientation of the object. Parameterizing the object, and numerically solving the resulting set of multivariable equations (minimization has to be performed over the spatial coordinates and the distributions of density and susceptibility), provides the levitation height and equilibrium orientation for arbitrary objects in arbitrary magnetic fields.

Simplifications of Eq. 4 allow analytical closed-form solutions that provide physical insight. The equilibrium levitation height h_0 will occur where $\frac{dU}{dh} = 0$. For a linearly varying magnetic field, the levitation height of the centroid of the object in the MagLev depends only on the average susceptibility $\bar{\chi}_o = \frac{1}{V}\int_V \chi_o(\vec{r})\, dV$ and the average density $\bar{\rho}_o = \frac{1}{V}\int_V \rho_o(\vec{r})\, dV$ of

the object, regardless of the shape and the distribution of the heterogeneities within the object. Thus, replacement χ_o with $\bar{\chi}_o$and ρ_o with $\bar{\rho}_o$ in Eq. 3 gives the levitation height of the centroid of an arbitrary object The SI contains the derivation).

The equilibrium orientation(s) at angle α will occur at the local minima of *U,* where $\frac{dU}{d\alpha} = 0$ and $\frac{d^2U}{d\alpha^2} > 0$. We choose a body-fixed coordinate system $\vec{p}(x'', y'', z'')$ aligned with a principal axes of the object, and fix the *x''*-axis to remain parallel to the *x'*-axis of the MagLev reference frame (we include the full derivation and a procedure to find this preferred reference frame in the SI). We proceed to analyze the rotation of the object around the *x'*-axis with the same convention as in the experiments and parameterize orientation as the angle α that $\vec{p}$ subtends with respect to the *z'*- axis. Equation 5 gives this energy for an object that is homogenous in susceptibility and density.

$$U(\alpha) = \beta \Delta\chi V {\lambda_z}^2 (1 - R) \sin^2 \alpha, \qquad (5)$$

In this equation, $\beta = \frac{2{B_0}^2}{\mu_0 d^2}$, ${\lambda_z}^2$ is the principle second moment of area along the *z''*-axis, and *R* is the ratio of the principle second moments of area along the *y''*- and *z''*- axes.

Fig. 3A shows a plot of Eq. 5 at representative values of *R.* For values of $R < 1$, $U(\alpha) \propto \sin^2 \alpha$, and the potential minima occur at $\alpha = 0^o$ and 180^o. For values of $R > 1$, $U(\alpha) \propto -\sin^2 \alpha \propto \cos^2 \alpha$, and the potential minima occur at $\alpha = 90^o$ and 270^o. All other values of α result in energies that lie within these extrema and are not stable. Thus, objects with uniform density will *only* orient with $\alpha = 0^o$ or $\alpha = 90^o$. This result rationalizes the experimental observations in Fig. 2. When R approaches 1, the linear theory predicts a flat energy landscape.

Adapting the analysis that led to Eq. 5 for nonlinear magnetic fields by retaining higher order terms in the expression for $\vec{B}$ provides solutions for the orientation of these objects (See SI).

We calculate the value of A_R^* at which it is energetically favorable for the objects to switch orientation from $\alpha = 0^o$ or $\alpha = 90^o$, and plot the results in Fig. 2C-F as a dashed line (See SI Appendix for full calculation.) Our calculations match our experimental results excellently. Furthermore, plotting α versus R results in the collapse of our data for all the shapes onto a master curve where the transition between orientations occurs at $R = 1$ (Fig. 3B).

Manipulating the Orientation of Objects by Rotating the MagLev Device. We used another Nylon screw (8.5 mm in length) to illustrate the process involved in manipulating — without contact with a solid surface — the orientation of an object suspended inside an entirely closed container of paramagnetic liquid. We controlled the orientation of the screw by rotating the MagLev device together with the container of paramagnetic liquid. The concentration of $MnCl_2$ was again 1.50 M, and thus the screw levitated at the center of the device (See Eq. 3.). Fig. 4 shows the orientation of the screw in the *y*-*z* plane when the device was rotated 360° counter-clockwise about the *x*-axis (the *z'*- axis rotated relative to the *z*- axis). For reference, we used a 30 × 22 mm cross as a background, keeping the cross fixed with respect to the laboratory frame of reference. The screw, suspended in solution, rotated in the lab frame of reference and tracked the angle of rotation of the magnets (Fig. 4B). Rotations about the other two axes resulted in similar outcomes (data not shown). We conclude that rotating (and translating) about the *x*-, *y*-, and *z*- axes allows arbitrary orienting and positioning of objects in three dimensions with respect to the laboratory frame of reference. Fig. S4 demonstrates that the orientation of the objects can also be manipulated by moving only the magnets, while keeping the container stationary — a

procedure that might be useful in certain situations: for example, when access to the oriented objects from the top of the container is desired.

Choosing a solution that has the same density as the object is important for contactless manipulation of objects by rotating the device. Fig. 4C shows the results when the density of the solution is lower than the density of the object (e.g., the same screw used in Fig. 4B). Rotating the device to 45^{o} caused the screw to translate towards the walls of the container, and eventually to contact the wall. Further rotation of the device to 90^{o} caused the screw, which was touching the container, to flip, and prevented its further manipulation. Although not shown here, it is rational to speculate that normal forces on an object, due to contact with a hard wall, might damage or deform soft, sticky, or fragile objects.

Why does using a solution of lower density cause the screw to contact the wall of the container? Recall that when the density of the solution is equal to the density of the object, the gravitational force acting on the object is zero (Eq. 1), and the center of volume of the object levitates at the center of the device (Eq. 3). When the density of the solution is less than that of the object, force balance requires that the object equilibrate at a smaller levitation height (the example shown in Fig. 4C), due to the non-zero gravitational force. Reversing the direction of the force vectors describes the situation for objects with a density higher than the solution, and the object equilibrates at a larger levitation height. Rotating the direction of the magnetic force (always acting along the z'-axis) with respect to the direction of the gravitational force (always acting along the z- axis) produces a component of the net force that acts perpendicular to the z-axis. The perpendicular component of the force, which increases in magnitude with increasing angles of rotation and reaches a maximum at $\theta=90^{o}$, causes the object to translate towards the wall to maintain static equilibrium.

It is clear that when the gravitational force is zero, the object remains fixed at the center of device. This configuration allows arbitrary rotations of the device without the object contacting the walls of the container. A practical means of matching the density of the liquid to an object of unknown density is to start with a concentrated solution of paramagnetic salt and progressively dilute the solution until the object levitates at the center of the device.

Manipulating the Orientation of Objects with External Magnets. Another method of controlling the orientation of objects, without contact with a solid surface, is by using external magnets to modify the magnetic field generated by the fixed coaxial magnets in the MagLev device. It is energetically favorable for the paramagnetic liquid in the container to respond to changes in the magnetic field by redistributing volume to occupy regions of locally high field strength. This movement of liquid will indirectly cause the displacement of levitating diamagnetic objects in the MagLev device.

We demonstrate this method by manipulating the orientation of a Nylon screw (2 cm in length) in the *x'-y'* plane of a MagLev device equipped with disc-shaped magnets (Fig. 5). We used circular magnets since this geometry resulted in a circularly symmetric field in the *x'-y'* plane. Thus, the screw does not have any preferred orientation in this plane. Magnets with shapes of lower symmetry, for example square and rectangular magnets, favor the orientation of the object along specific planes of symmetry, such as along the diagonals (Fig. S4) (27, 47). Fig. 5B shows an image of the screw viewed along the *x'-y'* plane of the device. A cross pattern affixed to the bottom magnet is provided as a guide to the eye. As expected, the long axis of the screw always oriented perpendicular to the *z'* axis while the head of the screw adopted a different orientation in the *x'-y'* plane each time the container was placed in the device (Fig. 5B shows just one such orientation).

We used a small cubic magnet (0.64 × 0.64 × 0.64 cm, magnetic field strength at the surface ~ 0.4 T) to generate, externally, a localized region of high magnetic field strength to manipulate the orientation of the head of the screw. We brought the small magnet to a distance of about two cm from the head of the levitating screw (the walls of the container prevented a closer approach of the magnet). The head moved away from the small magnet and came to rest after rotating ~ 45^{o} away from the surface of the external magnet. By moving the magnet around the exterior of the container, we oriented the head of the screw along the four principal axes of the cross (Fig. 5C). At each position, the screw remained at its new orientation even after the small magnet was moved away from the device. Furthermore, combinations of several external magnets allowed finer control of the orientation of levitating objects (Fig. S5).

Orienting Soft and Sticky Objects in MagLev. MagLev shows particular promise for manipulating and controlling the orientation of soft materials. As proof or principle, we used MagLev to manipulate objects fabricated out of hydrogels, elastomers, and colloids — three classes of materials with diverse technological applications.

Hydrogels have been used to fabricate actuators (15), soft robots (5, 9), and artificial tissues (6-8). For example, directed assembly of hydrogel strips and blocks laden with different cell-types is a promising method for engineering artificial tissues (6-8). Hydrogels used in biomimetic applications are soft (6-8), and tend to stick to surfaces due to the capillary action of the liquid film on the hydrogel surfaces. In Fig. 6A, we used MagLev in combination with an external magnet to orient a slab of poly(N-isopropylacrylamide) hydrogel; ordinarily, this material would deform or break when handled by a hard gripper (Young's modulus, E, of the hydrogel ~ 1000 Pa). We inserted the object into the MagLev device by gently releasing the hydrogel from the mold into the paramagnetic liquid. In the MagLev container, the object was

able to assume its natural shape, and the competing magnetic and gravitational forces acting on it determined its orientation. An external magnet allowed the control of the orientation of the sharp end of the hydrogel relative to the four principal axes of the cross.

In Fig. 6B, we controlled the orientation of a pneumatically actuated soft-gripper made out of the silicone elastomer EcoFlex. The gripper, a modular part of a larger soft robot assembly(48), deforms easily when subject to moderate forces and tends to adhere to surfaces due the low surface energy of cured EcoFlex. Rotating the magnets allowed control over the orientation of the gripping face with respect to the laboratory frame of reference. We envision that MagLev, with further development, could extend modular strategies for the assembly (48) of robots to materials that are softer than elastomers (e.g., hydrogels (9)).

Self-assembled granular and colloidal materials, held together by relatively weak physical bonds, are a class of soft or fragile condensed matter that show promise as stimuli-responsive materials and containers (11, 13, 14, 49-51). These materials, despite being composed predominantly of fluid, can adopt non-spherical shapes (i.e., they can demonstrate solid-like properties) due to the jamming of the colloidal particles on their surfaces (12, 51, 52). The capillary bonds that confer their solid-like properties are weak, and hence these solids have yield strengths on the order of γ/R ~ tens of Pa (53). The surface tension of the liquid is γ (N/m), and the radius of the object is R. Although such low yield strengths are sufficient to maintain the shape of the objects against gravity and thermal agitation, once fabricated, these objects cannot be manipulated with hard grippers without causing irreversible plastic deformation due to localized shear-melting of the jammed colloidal monolayer (53, 54). Fig. 6C shows control over the orientation of a non-spherical perfluorodecalin droplet covered with a jammed monolayer of 10-μm diameter polystyrene particles. We obtained the stable non-spherical peanut-like object by forcing two spherical particle-covered droplets to fuse by squeezing them mechanically.

MagLev thus allows active manipulation of self-assembled diamagnetic granular structures without requiring the use of magnetic or paramagnetic particles (11). All of the manipulations demonstrated here can also be performed on composite objects with metallic components (Fig. S6).

Conclusion

Previous works have shown that an object placed in a MagLev device orients reliably based on the distribution of density in the object (47). In this paper, we have demonstrated experimentally and theoretically that, for objects with a homogeneous density, the distribution of volume (i.e. shape) also plays a relevant role in determining the orientation of the object. As a result, we have shown that MagLev provides a method to *control* the orientation of objects (including objects that are soft or fragile) in three dimensions without contact, which may have implications for industrial applications such as automated assembly. The MagLev-based method for controlling the orientation of objects has a number of useful features. (i) It is non-damaging to fragile objects because it does not involve mechanical contact. (ii) It can flexibly orient objects of various shapes and a range of sizes. (iii) It can control the orientation of objects in three dimensions. (iv) It can control the orientation of objects inside an entirely closed container. (v) It is inexpensive. (vi) It does not require an external power source or any additional equipment to operate, beyond holders for the magnets. (vii) It can be made biocompatible with the use of chelated paramagnetic salts (45). (viii) Non-aqueous paramagnetic liquids (46) make it possible to use this method on moisture- or water-sensitive objects.

In its present form, this method also has several limitations. (i) MagLev, as we describe it here, operates best with materials with densities of ~ $1 < \rho < 3$ g/cm^3. It is well-adapted to

organic polymers, but less so to metals and heavier ceramics, although with higher field strengths and more dense paramagnetic liquids, it should also apply to more dense objects. (ii) MagLev does not enable control over the orientation of objects smaller than ~ ten micrometers in diameter because the magnetic and gravitational forces acting on these objects are insufficient to overcome Brownian motion, for the configuration and type of magnets used in this study.

These limitations aside, MagLev is compatible with a number of practical objects, such as plastic screws, polymeric objects, metal-polymer composites, soft hydrogels, elastomers and granular matter. As such, we expect that further development of the MagLev as a strategy for orientation and assembly of components will ultimately prove particularly useful in fields that require the manipulation and self-assembly of soft materials (e.g., components of soft robots (5, 9) or mechanically fragile components.

Materials and Methods

Full experimental details are provided in SI Materials and Methods.

Additional Information

This article contains supporting information online at [Filled by Editorial Staff]

Competing financial interests:

The authors declare no competing financial interests.

Acknowledgements

All aspects of this work relating to magnetic self-assembly were funded by the U.S. Department of Energy under award ER45852. A.K.E. acknowledges the Ford Foundation. A.B.S, S.T., S.S, acknowledge salary support from the Bill and Melinda Gates Foundation award # 51308. H.D.Y. acknowledges the A*STAR International Fellowship from the Singapore government. We thank Dr. A. Reina, and Dr. R.M.D. Nunes, for preliminary experiments and helpful conversations.

References

1. Horn BKP & Ikeuchi K (1984) The mechanical manipulation of randomly oriented parts. *Sci.Am.* 251(2):100-111.
2. Cappelleri DJ, Cheng P, Fink J, Gavrea B, & Kumar V (2011) Automated assembly for mesoscale parts. *IEEE Trans. Autom. Sci. Eng.* 8(3):598-613.
3. Schraft RD & Ledermann T (2003) Intelligent picking of chaotically stored objects. *Assem. Autom.* 23(1):38-42.
4. Shea K, Ertelt C, Gmeiner T, & Ameri F (2010) Design-to-fabrication automation for the cognitive machine shop. *Adv. Eng. Inform.* 24(3):251-268.
5. Fusco S*, et al.* (2014) An integrated microrobotic platform for on-demand, targeted therapeutic interventions. *Adv. Mater.* 26(6):952-957.
6. Gurkan UA, Tasoglu S, Kavaz D, Demirel MC, & Demirci U (2012) Emerging technologies for assembly of microscale hydrogels. *Adv. Healthc. Mater.* 1(2):149-158.
7. Tasoglu S*, et al.* (2013) Paramagnetic levitational assembly of hydrogels. *Adv. Mater.* 25(8):1137-1143.
8. Du YA, Lo E, Ali S, & Khademhosseini A (2008) Directed assembly of cell-laden microgels for fabrication of 3D tissue constructs. *Proc. Natl. Acad. Sci. U. S. A.* 105(28):9522-9527.
9. Nawroth JC*, et al.* (2012) A tissue-engineered jellyfish with biomimetic propulsion. *Nat. Biotechnol.* 30(8):792-797.
10. Xia YN, Gates B, Yin YD, & Lu Y (2000) Monodispersed colloidal spheres: Old materials with new applications. *Adv. Mater.* 12(10):693-713.

11. Dommersnes P*, et al.* (2013) Active structuring of colloidal armour on liquid drops. *Nat. Commun.* 4.

12. Subramaniam AB, Abkarian M, Mahadevan L, & Stone HA (2005) Non-spherical bubbles. *Nature* 438(7070):930-930.

13. Lee D & Weitz DA (2009) Nonspherical colloidosomes with multiple compartments from double emulsions. *Small* 5(17):1932-1935.

14. Shepherd RF*, et al.* (2006) Microfluidic assembly of homogeneous and janus colloid-filled hydrogel granules. *Langmuir* 22(21):8618-8622.

15. Keplinger C*, et al.* (2013) Stretchable, transparent,ionic conductors. *Science* 341(6149):984-987.

16. Murphy RJ (1982) U.S. Patent No. 4,310,964 A. Washington, DC: U.S.

17. Riley FJ (1996) *Assembly automation: A management handbook* (Industrial Press Inc., New York) 2 Ed.

18. Agrawal A, Sun Y, Barnwell J, & Raskar R (2010) Vision-guided robot system for picking objects by casting shadows. *Int. J. Robot. Res.* 29(2-3):155-173.

19. Buss M, Hashimoto H, & Moore JB (1996) Dextrous hand grasping force optimization. *IEEE Trans. Robot. Autom.* 12(3):406-418.

20. Yoshikawa T & Nagai K (1991) Manipulating and grasping forces in manipulation by multifingered robot hands. *IEEE Trans. Robot. Autom.* 7(1):67-77.

21. Ilievski F, Mazzeo AD, Shepherd RE, Chen X, & Whitesides GM (2011) Soft robotics for chemists. *Angew. Chem.-Int. Edit.* 50(8):1890-1895.

22. Martinez RV*, et al.* (2013) Robotic tentacles with three-dimensional mobility based on flexible elastomers. *Adv. Mater.* 25(2):205-212.

23. Brown E*, et al.* (2010) Universal robotic gripper based on the jamming of granular material. *Proc. Natl. Acad. Sci. U. S. A.* 107(44):18809-18814.

24. Bogue R (2012) Robots in the laboratory: a review of applications. *Ind. Robot* 39(2):113-119.

25. Pham DT & Yeo SH (1991) Strategies for gripper design and selection in robotic assembly. *Int. J. Prod. Res.* 29(2):303-316.

26. Bi ZM, Lang SYT, Shen W, & Wang L (2008) Reconfigurable manufacturing systems: the state of the art. *Int. J. Prod. Res.* 46(4):967-992.

27. Mirica KA, Shevkoplyas SS, Phillips ST, Gupta M, & Whitesides GM (2009) Measuring densities of solids and liquids using magnetic levitation: Fundamentals. *J. Am. Chem. Soc.* 131(29):10049-10058.

28. Kimura T, Mamada S, & Yamato M (2000) Separation of solid polymers by magneto-Archimedes levitation. *Chem. Lett.* (11):1294-1295.

29. Catherall AT, Lopez-Alcaraz P, Benedict KA, King PJ, & Eaves L (2005) Cryogenically enhanced magneto-Archimedes levitation. *New. J. Phys.* 7.

30. Waldron RD (1966) Diamagnetic levitation using pyrolytic graphite. *Rev. Sci. Instrum.* 37(1):29-35.

31. Simon I, Emslie AG, Strong PF, & McConnel RK (1968) Sensitive tiltmeter utilizing a diamagnetic suspension. *Rev. Sci. Instrum.* 39(11):1666-1671.

32. Evrard R & Boutry GA (1969) An absolute micromanometer using diamagnetic levitation. *J. Vac. Sci. Technol.* 6(2):279.

33. Beaugnon E & Tournier R (1991) Levitation of organic materials. *Nature* 349(6309):470-470.

34. Guevorkian K & Valles JM, Jr. (2006) Swimming Paramecium in magnetically simulated enhanced, reduced, and inverted gravity environments. *Proc. Natl. Acad. Sci. U. S. A.* 103(35):13051-13056.

35. Hirota N*, et al.* (2004) Magneto-Archimedes separation and its application to the separation of biological materials. *Physica B* 346:267-271.

36. Ikezoe Y, Hirota N, Nakagawa J, & Kitazawa K (1998) Making water levitate. *Nature* 393(6687):749-750.

37. Ikezoe Y*, et al.* (2002) Separation of feeble magnetic particles with magneto-Archimedes levitation. *Energ. Convers. Manage.* 43(3):417-425.

38. Kimura T (2003) Study on the effect of magnetic fields on polymeric materials and its application. *Polym. J.* 35(11):823-843.

39. Lyuksyutov IF, Lyuksyutova A, Naugle DG, & Rathnayaka KDD (2003) Trapping microparticles with strongly inhomogeneous magnetic fields. *Mod. Phy. Lett. B* 17(17):935-940.

40. Lyuksyutov IF, Naugle DG, & Rathnayaka KDD (2004) On-chip manipulation of levitated femtodroplets. *Appl. Phys. Lett.* 85(10):1817-1819.

41. Mirica KA, Phillips ST, Shevkoplyas SS, & Whitesides GM (2008) Using magnetic levitation to distinguish atomic-level differences in chemical composition of polymers, and to monitor chemical reactions on solid supports. *J. Am. Chem. Soc.* 130(52):17678-17680.

42. Valles JM, Lin K, Denegre JM, & Mowry KL (1997) Stable magnetic field gradient levitation of Xenopus laevis: Toward low-gravity simulation. *Biophys. J.* 73(2):1130-1133.

43. Winkleman A*, et al.* (2007) Density-based diamagnetic separation: Devices for detecting binding events and for collecting unlabeled diamagnetic particles in paramagnetic solutions. *Anal. Chem.* 79(17):6542-6550.

44. Yokoyama K, Hirota N, & Iwasaka M (2007) Separation of collagen by magneto-Archimedes levitation. *IEEE T. Appl. Supercon.* 17(2):2181-2184.

45. Winkleman A*, et al.* (2004) A magnetic trap for living cells suspended in a paramagnetic buffer. *Appl. Phys. Lett.* 85(12):2411-2413.

46. Bwambok DK*, et al.* (2013) Paramagnetic ionic liquids for measurements of density using magnetic levitation. *Anal. Chem.* 85:8442-8447.

47. Mirica KA, Ilievski F, Ellerbee AK, Shevkoplyas SS, & Whitesides GM (2011) Using magnetic levitation for three dimensional self-assembly. *Adv. Mater.* 23(36):4134-4140.

48. Kwok SW*, et al.* (2013) Magnetic assembly of soft robots with hard components. *Adv. Funct. Mater.*

49. Cayre OJ*, et al.* (2012) pH-responsive colloidosomes and their use for controlling release. *Soft Matter* 8(17):4717-4724.

50. Dinsmore AD*, et al.* (2002) Colloidosomes: Selectively permeable capsules composed of colloidal particles. *Science* 298(5595):1006-1009.

51. Herzig EM, White KA, Schofield AB, Poon WCK, & Clegg PS (2007) Bicontinuous emulsions stabilized solely by colloidal particles. *Nat. Mater.* 6(12):966-971.

52. Pieranski P (1980) Two-dimensional interfacial colloidal crystals. *Phys. Rev. Letts.* 45(7):569-572.

53. Subramaniam AB, Abkarian M, Mahadevan L, & Stone HA (2006) Mechanics of interfacial composite materials. *Langmuir* 22(24):10204-10208.

54. Datta SS, Shum HC, & Weitz DA (2010) Controlled buckling and crumpling of nanoparticle-coated droplets. *Langmuir* 26(24):18612-18616.

Figure Legends

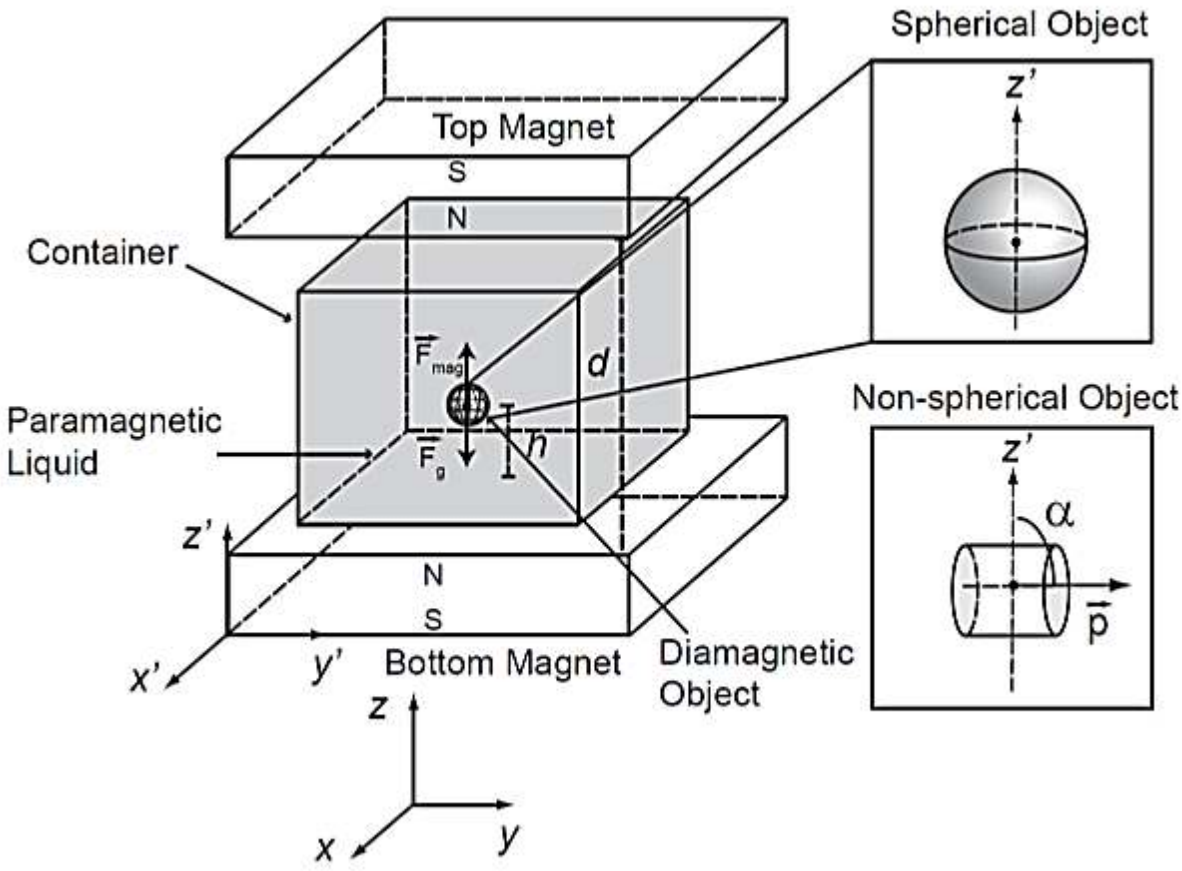

Fig.1 Scheme describing Magnetic Levitation. Two permanent magnets with like poles facing are arranged coaxially a distance, *d*, apart (the MagLev device). The laboratory fixed axes are *x*-, *y*-, and *z*-, and the axes fixed on the MagLev device are *x'*-, *y'*-, and *z'*-. A diamagnetic object (shown as a sphere) in a container containing paramagnetic liquid (dark gray), experiences a gravitational force $\vec{F}_g$ and a magnetic force $\vec{F}_{mag}$ when placed in the MagLev device. The schematic depicts the direction of the forces for an object of a higher density than the paramagnetic liquid. The direction of the vectors will be opposite for an object that is less dense than the liquid. When the two forces are in balance, the object levitates at a levitation height, *h*. **Inset.** A homogeneous spherical object has no unique plane of symmetry. To classify the orientation of non-spherical objects in the MagLev device (a cylinder is depicted here as an

example), we define a unit vector $\vec{p}$ (direction vector), taken typically to be along the long axis of the object. The angle subtended by $\vec{p}$ and the z'- axis (magnetic field axis) is α.

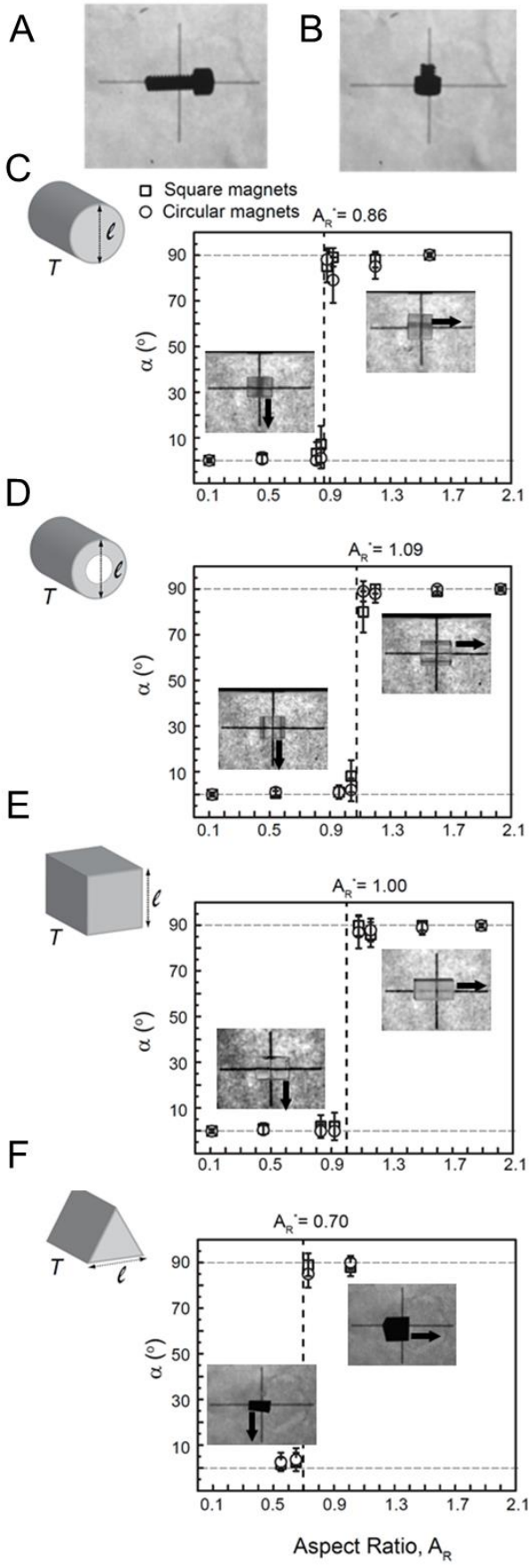
A
B
C
Square magnets
Circular magnets
$A_R^* = 0.86$
D
$A_R^* = 1.09$
E
$A_R^* = 1.00$
F
$A_R^* = 0.70$
T
ℓ
α (°)
Aspect Ratio, A_R

Fig. 2 Equlibrium orientations of non-spherical objects in MagLev. (A,B) A Nylon screw orients differently when the length of the shaft was reduced from 9.5 mm to 2.5 mm. (C-F) Plots of the the orientation of the objects (angle α) versus their aspect ratios $A_R=T/\ell$ (schematic). Each data point is an average of seven replicate objects. The error bars represent the standard deviation. The *x*-error bars are smaller than the data point. The dashed vertical line is the value of the critical aspect ratio, A_R^*, predicted by theory. The insets in each plot show representative images of objects levitating in the MagLev device. The black arrow indicates the direction of $\vec{p}$. The cross in the background is for reference, and the horizontal line in the cross measured 30 mm.

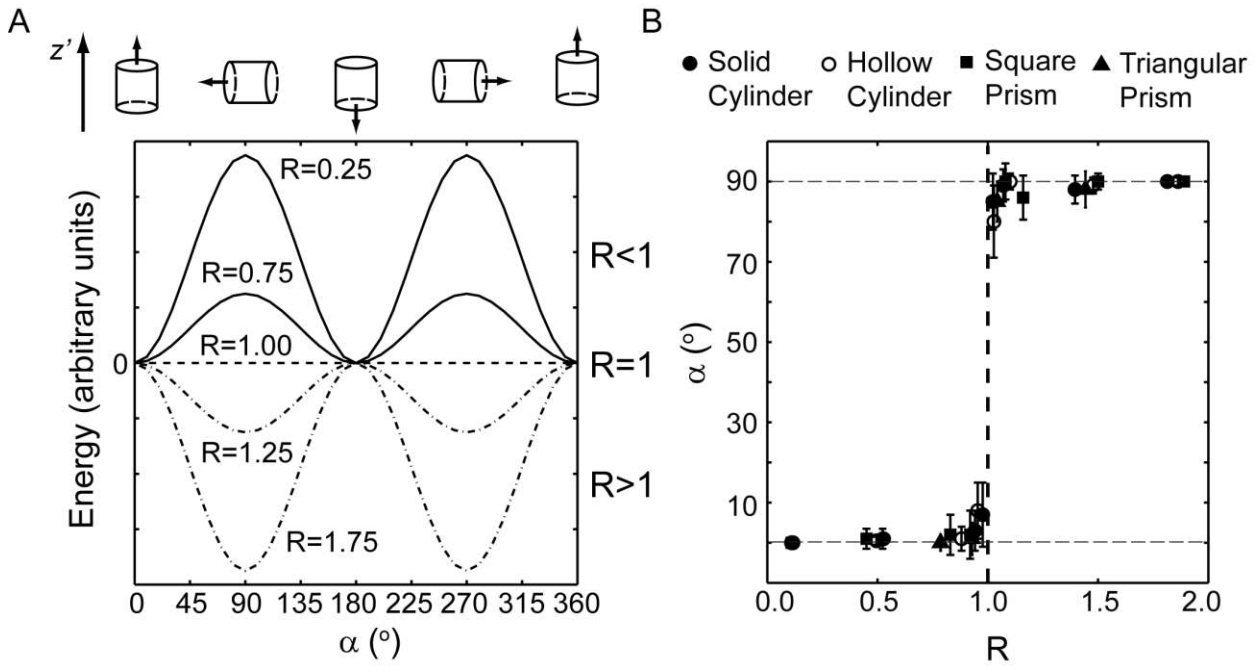

Fig. 3. Energy and orientation of objects in MagLev. (A) Plot of $U(\alpha) = \beta\Delta\chi V{\lambda_z}^2(1 - R)\sin^2\alpha$ (Eq. 5). R is the ratio of the second moment of area of the object and α is the angle that the $\vec{p}$ makes with respect to the *z'*-axis. For $R < 1$, continuous black line, the two (degenerate) minima in potential energy occur at α=90° and 270°. For $R > 1$, dashed and dot black line, the two (degenerate) minima in potential energy occur at α=0° and 180°. When R approaches 1, the linear theory predicts a flat energy landscape. Higher order nonlinear terms in the magnetic field become important and provide unique solutions (see SI). The schematic at the top of the plot shows the orientation of the object with respect to the *z'*. (B) Plot of α versus *R* fpr the experimental objects in Figure 2. All the data collapses onto a master curve with the transition in orientation at *R=1*.

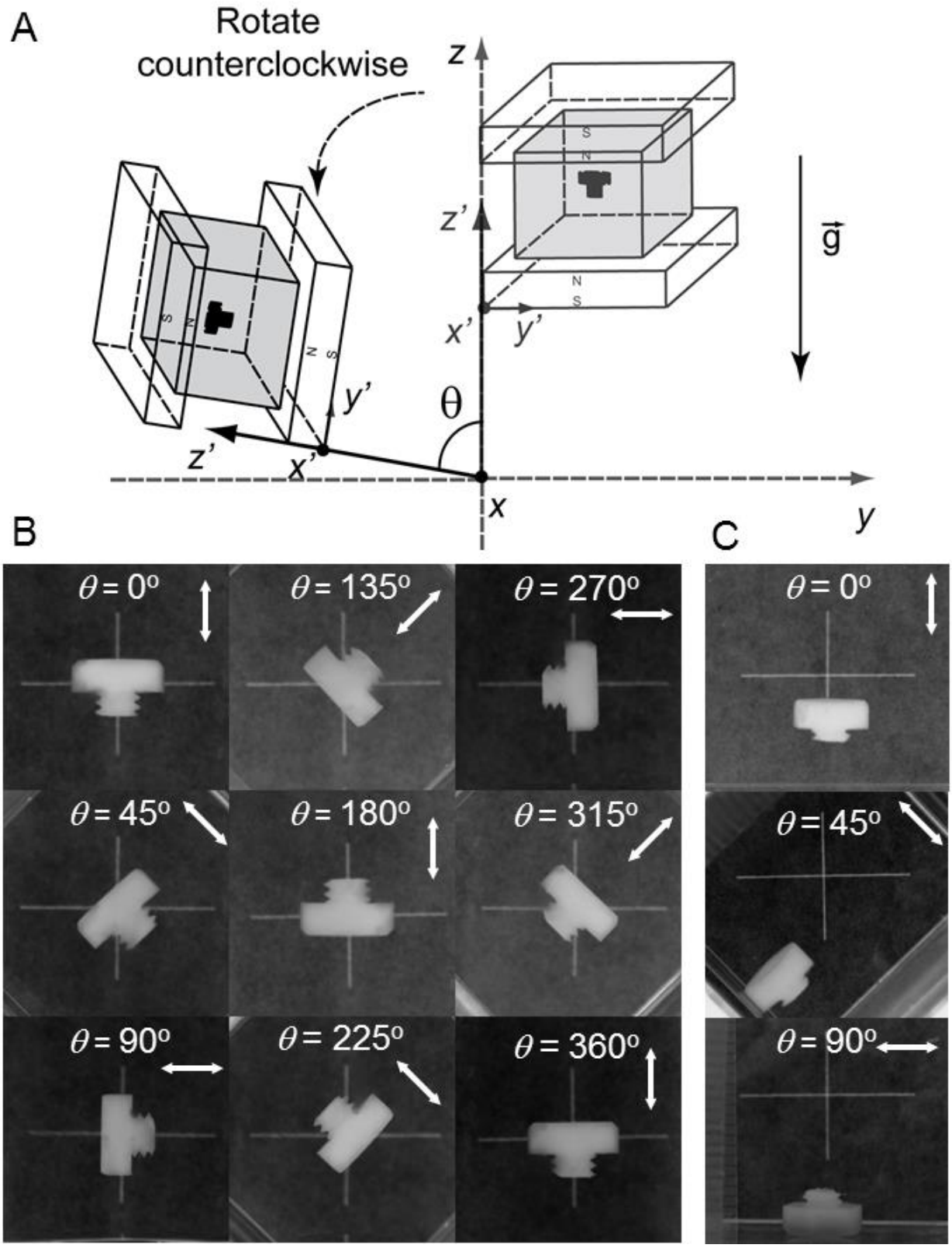
A
Rotate
counterclockwise
z
z'
x'
y'
θ
x
y
g
S
N
N
S
B
θ = 0°
θ = 135°
θ = 270°
θ = 45°
θ = 180°
θ = 315°
θ = 90°
θ = 225°
θ = 360°
C
θ = 0°
θ = 45°
θ = 90°

Fig. 4. Controlling the orientation of a levitating object in laboratory space by rotating the MagLev device. (A) Schematic of the experimental setup. We rotated the MagLev device with the container containing the screw anti-clockwise about the *x*-axis. The laboratory fixed axes are labeled *x*-, *y*-, and *z*- with the x-axis coming out of the page. The axes fixed on the device are labeled *x'*-, *y'*-, and *z'*- with the x'-axis coming out of the page. Gravity is positive downwards. θ is the angle that the *z'*- axis makes relative to the *z*- axis. (B) Experimental images taken along the *y*-*z* plane of a Nylon screw (8.5 mm in length) in the MagLev. We kept the cross in the background fixed relative to the laboratory. The screw tracks the position of the magnets, rotating a full 360^{o} with respect to the laboratory frame of reference. The white double headed arrows indicate the orientation of the axis of the magnetic field gradient. (C) Similar rotations caused the screw to translate and contact the wall of the container when the density of the screw was greater than the density of the solution. Further rotations caused the screw to flip orientation. For scale, the horizontal line in the cross is 30 mm.

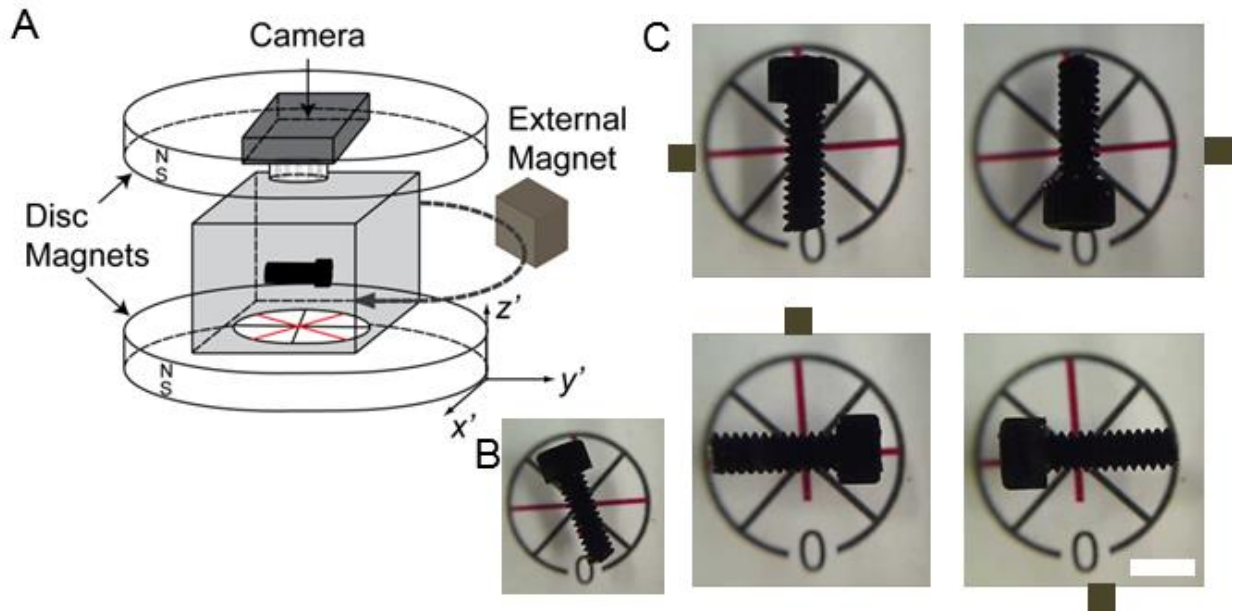

Fig. 5. Manipulating the orientation of an object in the *x'-y'* plane of a MagLev device with an external magnet. (A) Schematic of the experimental setup. We levitated a black Nylon screw in a MagLev device equipped with disc-shaped magnets. A webcam glued to the top magnet imaged the position of the screw. A crosshatch pattern glued to the bottom magnet served as a guide to the eye. Due to the cylindrical symmetry of the magnetic field, the long-axis of the screw does not have a preferred orientation in the *x'-y'* plane. The image in (B) shows one of the orientations the screw adopts when placed in the device. We moved an external magnet close to the screw to align the screw head along the red lines of the pattern. (C) Experimental images of the screw aligned along the pattern. The brown square indicates the approximate position of the external magnet. We did not monitor the movement of the screw in the other planes of the device. Scale bar 5 mm. Also see Fig. S5 for images taken along the z'-y' plane of a screw being manipulated with external magnets.

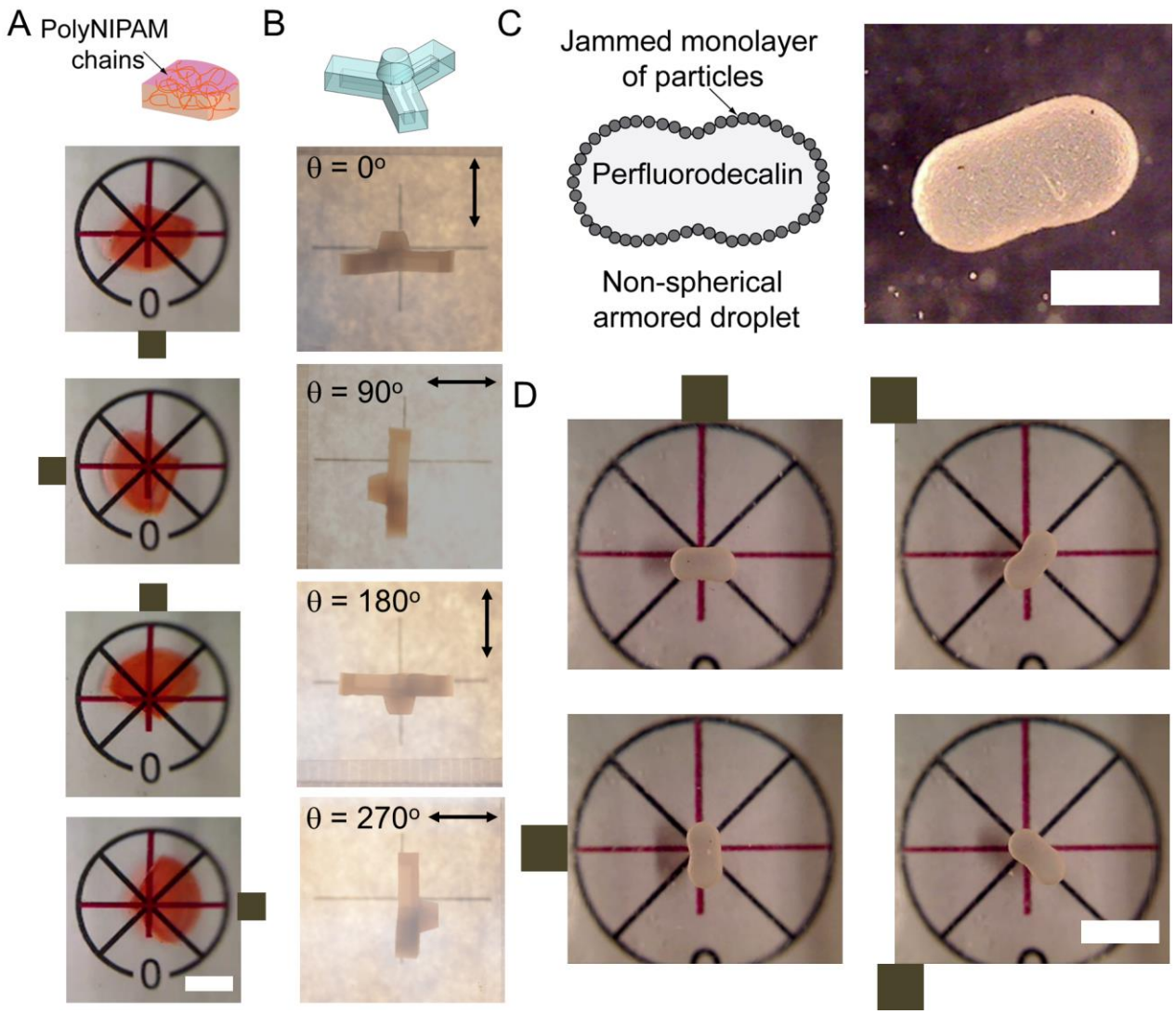

Fig. 6. Manipulation of soft, sticky, and easily deformable objects. (A) Photographs along the *x'-y'* plane showing control of the orientation of a PNIPAM hydrogel using external magnets. We used the same experimental setup as in Fig. 4. The sharp end of the hydrogel was made to point in the four principal axis of the cross pattern. The brown square indicates the approximate position of the external magnet. The hydrogel levitated stably in each position after we withdrew the external magnet. (B) Images along the *z'-y'* plane of a soft gripper component made out of Ecoflex 0030. The orientation of the gripping face was changed with respect to the laboratory

frame of reference by rotating the magnets. The black double headed arrows indicate the orientation of the axis of the magnetic field gradient, and θ is the angle of rotation of the magnets with respect to the *z*-axis. (C) Schematic and picture of an armored droplet. The droplet despite being composed predominantly of liquid, adopts a stable peanut shape due to the jamming of the polystyrene particles on its interface. (D) We controlled the orientation of the armored droplet with respect to the cross pattern by using an external magnet. The manipulation of the position of the object with MagLev did not deform this soft solid. Scale bars (A) 5 mm (B) the horizontal line of the cross is 30 mm. (C) 2 mm (D) 5 mm.

Supporting Information

Subramaniam et al.

SI Materials and Methods

Materials. We purchased manganese (II) chloride tetrahydrate (ACS Reagent Grade), perfluorodecalin (95 % pure), Allura Red AC (dye content 80 %) from Sigma Aldrich. Polystyrene particles were purchased from Invitrogen. Heavy Liquid was purchased from GeoSciences Inc. Polymeric components, such as poly(methyl methacrylate) (PMMA), polytetrafluoroethylene (Teflon) and polyoxymethylene (Delrin), were purchased from McMaster-Carr and custom machined: PMMA sheets with a thickness $\ell = 6.35$ mm, rods with a diameter $\ell = 6.35$ mm, tubes with an outer diameter $\ell = 6.35$ mm and inner diameter of 5.56 mm were cut into rectangular, circular, and annular blocks with different thickness, T; Delrin and PMMA sheets were cut into equilateral triangular prisms ($\ell = 6.67$ mm) with different T. Polyamide (Nylon 6/6) screws (2 cm in length) were purchased from McMaster-Carr.

Levitation of Objects in MagLev. We used commercially available NdFeB magnets — square magnets (5.0 × 5.0 × 2.5 cm) or disc magnets (4.8 cm in diameter, 2.5 cm thick), which are capable of providing surface fields of ~ 0.4 T. We levitated objects in an aqueous solution of $MnCl_2$ in a rectangular glass container (4.5 × 3.0 × 4.5 cm). We adjusted the concentration of $MnCl_2$ to yield a solution that had a density that was similar to that of the object so that the object levitated close to the center of the device. We sonicated the solution for one minute to remove air bubbles. After waiting a minimum of three minutes, to allow the object to levitaite to

its equilbrium height and orientation, we took an image of the objects in the device, using a Nikon DS-50 digital camera. We measured the orientation angle, α, from the photographs using ImageJ (NIH Bethesda). We used a digital angle indicator (McMaster-Carr, accuracy of 0.01°) when rotating the device.

Fabrication of Armored Droplets. We spread a monolayer of polysytrene particles onto an air/water interface by adding dropwise a suspension of polystrene particles in ethanol. The ethanol spread on the water surface and evoporated, thus depositing the particles on the surface. Once a complete monolayer had formed, we added perfluorodecalin dropwise onto the surface of this monolayer. The perfloruodecalin formed a lens-shaped drop and eventually, with additional volume, overcame the surface tension of the water and penetrated the surface of the liquid, and sank. Perfluorodecalin has a density higher than water (ρ=1.95 g/cm^3). The droplet picked up a jammed monolayer of particles from the water surface. These particles were trapped at the interface of the perfluorodecalin droplet and did not desorb. We produced two coated droplets that we then fused to form the peanut shaped object by squeezing the droplets between two glass plates(12). We then added $MnCl_2$ and a commercial water-based density matching liquid (Heavy Liquid, ρ=2.85 g/cm^3, Geoliquids Inc) and levitated the non-spherical droplet in the MagLev device.

SI Figures

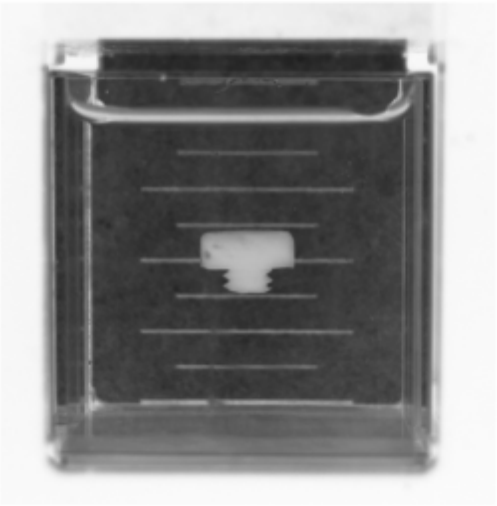

Fig. S1. The orientation of objects does not depend on its levitation height in the MagLev device. We imaged the levitating Nylon screw along the *y*-*z*- plane. We progressively increased the density of the paramagnetic medium by adding sucrose, while keeping [$MnCl_2$] constant at 1.0 M. The orientation of the screw did not change with levitation height. The distance between the lines in the ruled scale in the background is 5 mm.

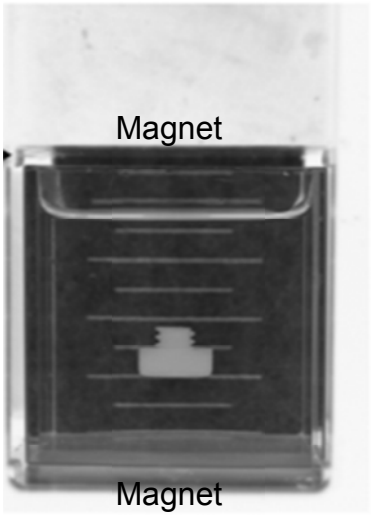
Magnet
Magnet


Magnet
Magnet

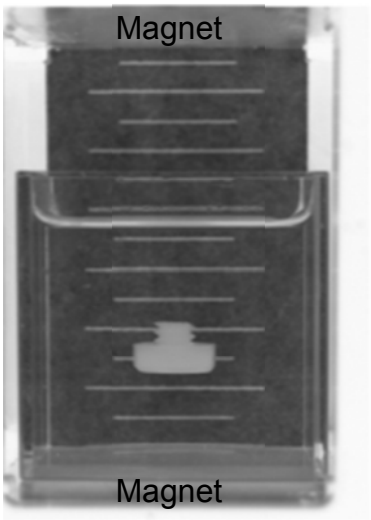
Magnet
Magnet

Fig. S2. The orientation of objects is insensitive to the separation distance between the magnets. We imaged the levitating Nylon screw along the *y*-*z*- plane. The separation distance between the top and bottom magnets: (from top to bottom) 45 mm, 55 mm, and 65 mm. The screw was levitated in 1.0 M $MnCl_2$ solution containing sucrose. The orientation of the screw did not change. The distance between the lines in the ruled scale in the background is 5 mm.


0
0
0

Fig. S3. Equilibrium orientation of objects in the *x'-y'* plane of the MagLev with square magnets. The top image shows the cross pattern that we used as a guide to the eye, the straight black lines in the pattern were aligned along the diagonals of the magnet. We allowed the hollow PMMA cylinder to equilibrate for 3 minutes before imaging. We then perturbed the cylinder by moving the container out of the device several times. The cylinder orients along the diagonals of the magnet. The behavior of the cylinder is expected based on the location of the minima in the magnetic field in this plane. Scale bar 5 mm.

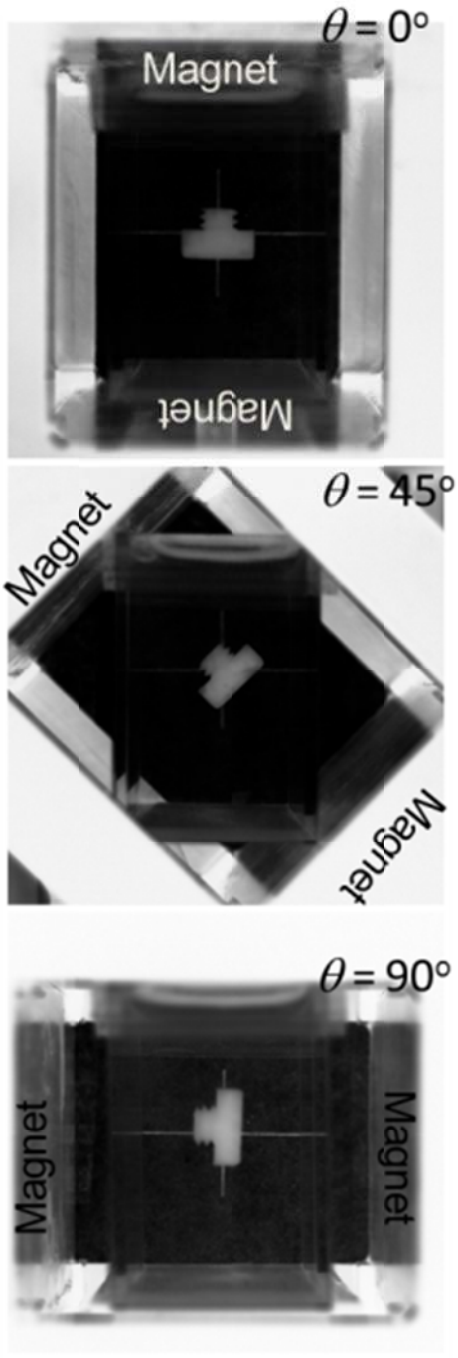
θ = 0°
Magnet
Magnet
θ = 45°
Magnet
Magnet
θ = 90°
Magnet
Magnet

Fig. S4. Keeping the container stationary while rotating the device as a means of manipulating the orientation of objects. We placed the container containing the screw and the paramagnetic liquid on a pedestal. We then rotated the MagLev device with respect to the container. The object tracked the position of the magnets. The cross in the background was fixed relative to the laboratory frame of reference. With this configuration, the top of the container remained open and accessible, allowing external grippers, for example, to retrieve the oriented objects. For scale, the horizontal line in the cross is 30 mm.

A

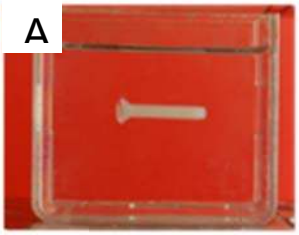

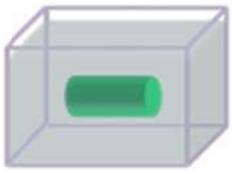

B

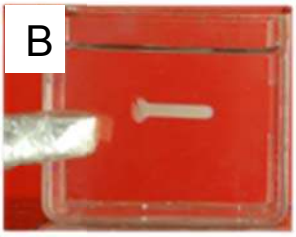

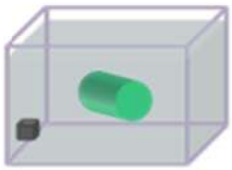

C

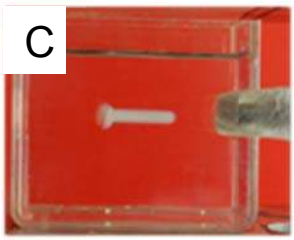

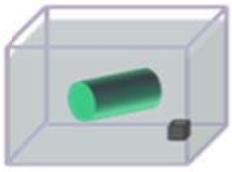

D

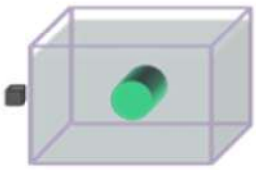

E

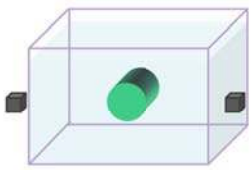

F

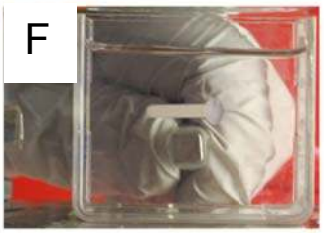

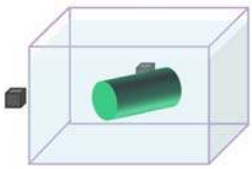

Fig. S5. Manipulating the orientation of an object in the *xy*- plane with an external magnet. (A) Initial orientation of a Nylon screw (2 cm in length) levitating in the MagLev device. The orientation of the screw was controlled by using (B-D) one or (E-F) two external magnet(s) . The screw remained in its new position orientation after the magnet(s) was/were removed. Schemes on the right show the orientation of the objects.

A

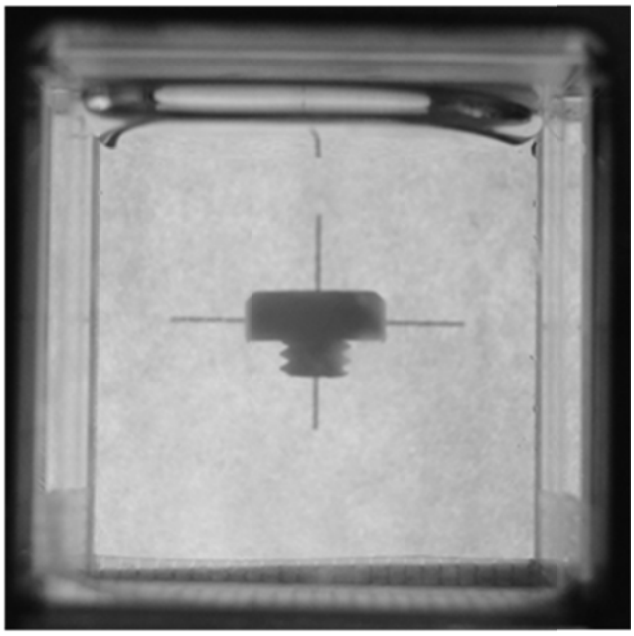

B

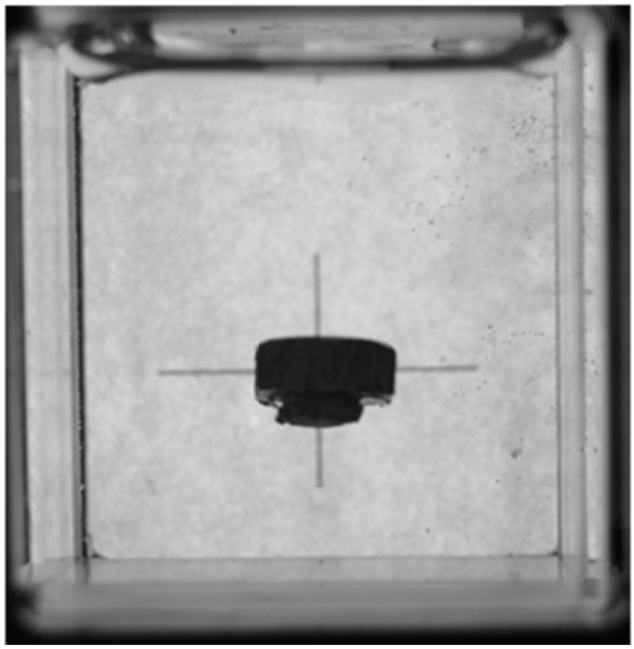

Fig. S6 Manipulation of objects with metallic or paramagnetic components. (A) A Nylon screw levitating in the MagLev device. The paramagnetic solution is [$MnCl_2$] = 1.0 M. (B) The same screw wrapped in aluminum foil and levitating in the device. The orientation of the object did not change.

SI Text

In our experiments, we observed that objects of homogeneous density and anisotropic shape levitating in a MagLev device moved to a stable levitation height away from the surface of the magnets and adopted a stable orientation with respect to the magnetic field. The orientation of the object depended on the object's shape and its aspect ratio. As the aspect ratio of the object was increased, we observed that the objects changed orientation sharply at a critical aspect ratio.

In the following sections, we present a general theory for the orientation and levitation of arbitrary objects in MagLev. The layout of the SI is as follows. In section I, we obtain an analytical closed form approximation of the magnetic field in a MagLev device. In Section II, we derive the potential energy of an arbitrary object in a MagLev device and find expressions for the equilibrium height and equilibrium orientation of the object. We conclude: (i) the levitation height of the centroid of an object depends only on its average density and its average susceptibility. The levitation height does not depend on the the distribution of these quantities within an object. This result greatly simplifies calculations for objects of heterogeneous density and/or magnetic susceptibility; (ii) a homogeneous object has only two potential stable configurations in the MagLev. The configuration that is preferred (i.e. of lowest potential energy) depends only on the ratio of second moments of area of the object. This result is consistent with a torque balance, but is more general and proves that the levitating object does not have any metastable orientations. In section III, we calculate the potential energy of the levitating objects used in experiments and obtain analytical predictions for the critical aspect ratio, A_R at which transitions in orientation occur. The theoretical values are in excellent agreement with experiments.

1 Expression for the Magnetic Field in the Magnetic Levitation Device

We assume that the MagLev device is stationary with respect to the laboratory frame of reference. Thus the fixed coordinates (i.e., the laboratory frame of reference), the x-,y-,z-axes, as defined in the main text, is always coincident with the body-fixed x'-,y'-,z'- axes of the MagLev device. To simplify the notation, we equate these two coordinates and define the "MagLev frame of reference" as $\vec{r} = (x, y, z)$.

The Maglev device consists of two coaxial circular or square magnets with like poles facing set a distance d apart. We choose the z axis (unit vector $\mathbf{e}_z$) to be the axis of symmetry and define the upper surface of the bottom magnet to be $z = 0$ and the lower surface of the top magnet to be at $z = d$. This simple configuration between the two magnets sets up a rather complicated magnetic field that is a function of axial and radial positions.

In our experiments we find that the orientation of the object in the plane perpendicular to the surface of the magnets is independent of the shape of the magnets. Thus, to simplify the analysis, we consider the radially symmetric case, and let the lateral extent of the magnetic field to be R. The axial symmetry allows the expression of the magnetic field in the volume between the magnets $-R \leq x \leq R$, $-R \leq y \leq R$ and $0 \leq z \leq d$, in cylindrical coordinates, approximately as a field that is a function of z and $\rho = \sqrt{x^2 + y^2}$, $\mathbf{B}(\rho, z)$. Note that the term ρ used in this section is different from the use of ρ for the mass density. For ρ used to refer to mass density we always have a subscript to refer to the object.

We next obtain an approximation for the field, $\mathbf{B}(x, y, z)$, between two magnets in the absence of the paramagnetic medium. Solving Maxwell's equations yields the magnetic field - this is however complicated to attempt analytically. The field generated by two-loops of wire of radius R through which a current I flows, arranged in the

anti-Helmholtz configuration yields to leading order:

$$B_z = 3I\mu_o\left(\frac{d}{2}R^2\right)\left[(\frac{d}{2})^2+R^2\right]^{-\frac{5}{2}}\left(z+\frac{d}{2}\right)+.... \quad (1)$$

$$B_\rho = -\frac{3}{2}I\mu_o\left(\frac{d}{2}R^2\right)\left[(\frac{d}{2})^2+R^2\right]^{-\frac{5}{2}}\rho+... \quad (2)$$

Here, μ_o is the permeability of free space. The region of field minimum is at the center of the device equidistant from the surface of the magnets. The field is maximum at the surface of the magnets, i.e. at $z = 0$ and d, and the magnitude of B_o can, in principle, be a function of z and ρ. A single permanent magnet can be modeled as an infinite number of loops extending from $R = 0$ to $R = R_m$, where R_m is the radius of the magnet. Thus, integrating, and keeping only leading order terms, the field due to permanent magnets in the anti-Helmholtz configuration is expected to have the form
$B_z \approx \left[\int_0^{R_m} 3I\mu\left(\frac{d}{2}R^2\right)\left[(\frac{d}{2})^2+R^2\right]^{-\frac{5}{2}}\,dR\right]\left(z+\frac{d}{2}\right)$ which on rearranging yields approximate expressions

$$B_z = B_{o,z}\left(1-2\frac{z}{d}\right), \quad \text{and} \quad (3)$$

$$B_\rho = B_{o,\rho}\left(\frac{\rho}{R}\right) \quad (4)$$

Thus, the field is approximately

$$\mathbf{B}^o(x,y,z) \approx B_{o,z}\left(1-2\frac{z}{d}\right)\mathbf{e}_z+\frac{1}{\sqrt{2}}B_{o,\rho}\left(\frac{\rho}{R}\right)\mathbf{e}_x+\frac{1}{\sqrt{2}}B_{o,\rho}\left(\frac{\rho}{R}\right)\mathbf{e}_y. \quad (5)$$

The magnetic flux lines are perpendicular close to the surface of the magnets but curve appreciably at the center. Thus, although the magnetic field is zero at the point equidistant between the magnets, this is also a point of inflexion of the flux lines. When a paramagnetic liquid, of magnetic susceptibility χ_m, is introduced between the magnets, the magnetic field will change. To leading order, one may approximate the field by the linear

term in z - this is the Taylor series expansion about the point $\rho = 0$ where only the term due to the geometric symmetries of the two-magnet configuration is retained. Thus (consistent with Mirica et. al. (2)) we write approximately

$$\mathbf{B}(x, y, z) \approx B_o \left(1 - 2\frac{z}{d}\right) \mathbf{e}_z. \tag{6}$$

For a linear variation in z, B_o is constant.

2 Equilibrium Orientation and Position of an Object of Arbitrary Shape in a Linearly Varying Magnetic Field

2.1 Total Energy

Consider a dielectric object, of volume V, in an paramagnetic medium suspended in a uniform magnetic field defined in (6). The object has a magnetic susceptibility $\chi_o(\vec{r})$ and density $\rho_o(\vec{r})$. These quantities may vary as a function of position, parametrized by the vector $\vec{r} = (x, y, z)$, within the object. The magnetic susceptibility of the medium is χ_m. To simplify calculations, we take advantage of the symmetry of the magnetic field and define the origin, O, of the MagLev frame of reference at $z + d/2$. Therefore z is measured relative to the center of the device (where $B = 0$) and $\mathbf{B} = \frac{2B_o}{d} z\mathbf{e}_z$. Since both $\chi(\vec{r})_o \ll 1$ and $\chi_m \ll 1$, the warping of the field is negligible; the object does not significantly modify the shape of the magnetic field lines. This assumption is true for most diamagnetic objects and paramagnetic media. Equation (7) gives the potential energy density due to the magnetic field within the volume of the object.

$$u_{mag} = -\frac{1}{2}\frac{\Delta\chi(\vec{r})}{\mu_0}\mathbf{B}\cdot\mathbf{B} = -\frac{\Delta\chi(\vec{r})}{2\mu_0}\left(\frac{2B_s}{d}z\right)^2 = -\frac{2\Delta\chi(\vec{r})B_0^2}{\mu_0 d^2}z^2$$
$$= \beta\Delta\chi(\vec{r})z^2 \tag{7}$$

In this equation, $\Delta\chi(\vec{r}) = \chi_o(\vec{r}) - \chi_m$, and we have defined the constant $\beta = -\frac{2B_0^2}{\mu_0 d^2}$. Equation (8) gives the potential energy density due to the gravitational field within the volume of the object.

$$u_{grav} = \Delta\rho(\vec{r})gz, \tag{8}$$

Integrating the energy density over the volume of the object provides the potential energy of the system. (Equations (9) and (10)).

$$U_{mag} = \int_V u_{mag}dV = \beta\int_V \Delta\chi(\vec{r})z^2 dV \tag{9}$$
$$U_{grav} = \int_V u_{grav}dV = g\int_V \rho(\vec{r})z dV \tag{10}$$

In these equations, dV is the volume element in the MagLev frame of reference. The total energy of the MagLev system is $U = U_{mag} + U_{grav}$.

We next define a body-fixed frame of reference for the object, with origin O'. Translation and rotation of the object within the MagLev frame of reference can be described relative to this "object frame of reference". The object frame of reference is chosen arbitrarily (at first). We will provide in the subsequent sections a method to find the ideal reference frame that simplifies calculations.

Within this object frame of reference, we define $\vec{r'} = (x', y', z')$ to be the coordinates. Since the magnetic field in our approximation only varies in z, we take the origin O' to be along the z' axis. Any rotation of the object frame of reference in the MagLev frame of

reference can be described as a rotation by an angle α around some axis defined by $\mathbf{e}_u = (\sin\theta\cos\phi, \sin\theta\sin\phi, \cos\theta)$. We use spherical coordinates to describe the MagLev frame of reference: θ is the declination angle from z, and ϕ is the azimuthal angle measured from x. The axis of rotation will always lie in the xy-plane such that $\theta = \pi/2$ and $\mathbf{e}_z = (\cos\phi, \sin\phi, 0)$. A rotation by an angle α about the unit vector $\mathbf{e}_u$ can be represented by the rotation matrix in Equation (11).

$$A = \begin{pmatrix} \cos\alpha + (1-\cos\alpha)\cos^2\phi & (1-\cos\alpha)\cos\phi\sin\phi & \sin\alpha\sin\phi \\ (1-\cos\alpha)\cos\phi\sin\phi & \cos\alpha + (1-\cos\alpha)\sin^2\phi & -\cos\phi\sin\alpha \\ -\sin\alpha\sin\phi & \cos\phi\sin\alpha & \cos\alpha \end{pmatrix} \tag{11}$$

Any configuration of the object in the MagLev can be treated as a pure rotation by A of the original arbitrarily chosen configuration (which may not correspond to the minimal energy configuration of the object) plus a vertical translation $\vec{h} = (0, 0, h)$.The coordinate transformation from the object frame of reference to the MagLev frame of reference is given by Equation (12).

$$\vec{r} = A\vec{r'} + \vec{h}. \tag{12}$$

Since the energy only depends on z, we need only to find $z = \mathbf{e}_z \cdot \vec{r}$, which reduces to Equation (13).

$$\begin{aligned} z &= \mathbf{e}_z \cdot \left(A\vec{r'} + \vec{h}\right) = (\mathbf{e}_z A)\,\vec{r'} + \mathbf{e}_z \cdot \vec{h} \\ &= \begin{pmatrix} -\sin\alpha\sin\phi \\ \sin\alpha\cos\phi \\ \cos\alpha \end{pmatrix} \cdot \begin{pmatrix} x' \\ y' \\ z' \end{pmatrix} + h \\ &= -x'\sin\alpha\sin\phi + y'\sin\alpha\cos\phi + z'\cos\alpha + h \end{aligned} \tag{13}$$

Using Equation (13) we re-write the magnetic and gravitational potential energies in the object frame of reference.

$$U_{mag} = \beta \int_{V'} \Delta\chi(\vec{r}) \left(-x' \sin\alpha \sin\phi + y' \sin\alpha \cos\phi + z' \cos\alpha + h\right)^2 dV' \tag{14}$$

$$U_{grav} = g \int_{V'} \Delta\rho(\vec{r'}) \left(-x' \sin\alpha \sin\phi + y' \sin\alpha \cos\phi + z' \cos\alpha + h\right) dV'. \tag{15}$$

The behavior of U will depend on the zeroth, first, and second moments of the functions $\Delta\chi(\vec{r})$ and $\Delta\rho(\vec{r'})$ defined on the volume V' of the object. Expansion of these integrals will result in many terms. Choosing an appropriate object frame of reference (we call this frame of reference the "principal frame of reference") however, will result in many terms vanishing. We now proceed to describe a procedure for finding the principal frame of reference.

2.2 Moments of a Function

Consider an arbitrary object with volume V defined in an object frame of reference O' with body-fixed coordinates $\vec{r}' = (x', y', z')$. We define a general scalar function $f(x', y', z')$ inside the object, and $f = 0$ everywhere outside the object (Fig. 1). The moments of this general function $f(x', y', z')$ is given by Equation (16).

$$M_f^{ijk} = \int_{V'} x'^i y'^j z'^k f(x', y', z') dV'. \tag{16}$$

The center of f, in Cartesian coordinates, which we define as $\left(\bar{x}'_f, \bar{y}'_f, \bar{z}'_f\right)$ is given by

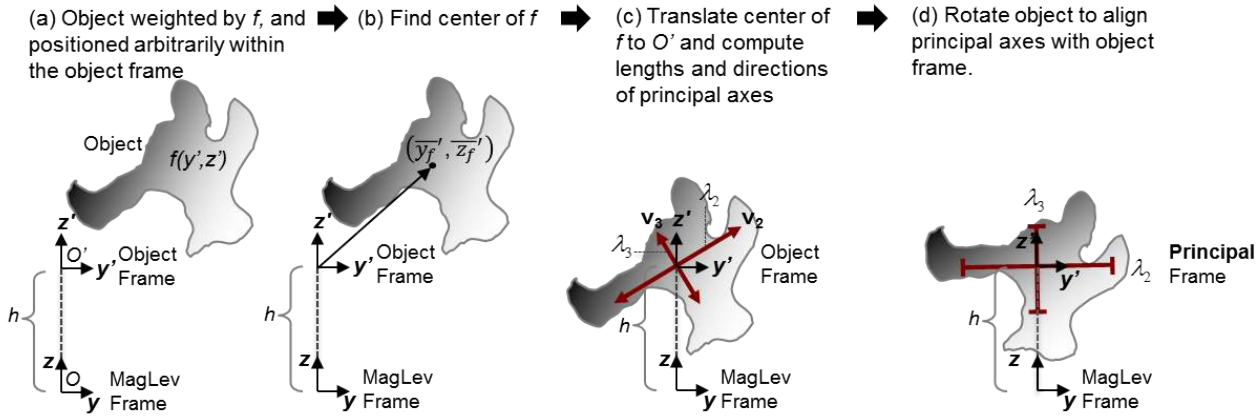

Figure S7: Procedure for finding the principal frame of reference of an arbitrarily oriented object in the MagLev. For clarity, we only show a 2D cross section of the object. Analyzing the orientational potential energy in the principal frame simplifies calculations.

Equations (17-19).

$$\bar{x}'_f = \frac{\int'_V x' f(x',y',z')dV'}{\int'_V f(x',y',z')dV'} = \frac{M_f^{100}}{M_f^{000}} \tag{17}$$

$$\bar{y}'_f = \frac{\int'_V y' f(x',y',z')dV'}{\int'_V f(x',y',z')dV'} = \frac{M_f^{010}}{M_f^{000}} \tag{18}$$

$$\bar{z}'_f = \frac{\int'_V z' f(x',y',z')dV'}{\int'_V f(x',y',z')dV'} = \frac{M_f^{001}}{M_f^{000}} \tag{19}$$

For example, if $f = const$, then $M_0^{000} = V'$ and $(\bar{x}', \bar{y}', \bar{z}')$ is the geometric centroid of the object. If $f = \chi(x',y',z')$, then $M_\chi^{000} = \int \chi(x',y',z')dV' = \bar{\chi}V'$, and $\left(\bar{x'}_\chi, \bar{y'}_\chi, \bar{z'}_\chi\right)$ is the center of susceptibility. If $f = \rho(x',y',z')$, then $M_\rho^{000} = \bar{\rho}V'$, and $\left(\bar{x'}_\rho, \bar{y'}_\rho, \bar{z'}_\rho\right)$ is the center of mass.

To find the principal axes and orientation of the object, we define the second order central moments of the object μ_f^{ijk} (Equation (20)).

$$\mu_f^{ijk} = \frac{M_f^{ijk}}{M_f^{000}} - \bar{x'}_f^{\,j} \bar{y'}_f^{\,j} \bar{z'}_f^{\,k} \tag{20}$$

We construct the covariance matrix of the function f (Equation (21)).

$$cov[f(x',y',z')] = \begin{bmatrix} \mu_f^{200} & \mu_f^{110} & \mu_f^{101} \\ \mu_f^{110} & \mu_f^{020} & \mu_f^{011} \\ \mu_f^{101} & \mu_f^{011} & \mu_f^{002} \end{bmatrix} \tag{21}$$

The covariance matrix allows calculation of the length and direction of the three principal axes of the object. The eigenvectors $(\mathbf{v_1}, \mathbf{v_2}, \mathbf{v_3})$ of the covariance matrix correspond to the principal axes of the object, weighted by the function f(x',y',z'). The eigenvalues $(\lambda_1^2, \lambda_2^2, \lambda_3^2)$ correspond to the squared length of the three principal axes. By constructing a rotation matrix $Q = [\mathbf{v_1 v_2 v_3}]$ composed of the eigenvectors, we can perform a change of coordinates $\vec{r}' \rightarrow Q\vec{r}'$ that will rotate the object such that its principal axes are parallel to the axes of the MagLev frame of reference.

If we translate $\left(\bar{x}'_f, \bar{y}'_f, \bar{z}'_f\right)$ to O', then $\bar{x}'_f = \bar{y}'_f = \bar{z}'_f = 0$, and $M_f^{100} = M_f^{010} = M_f^{001} = 0$. If we also rotate the object frame of reference by applying Q, then $\mathbf{v_1}$ will be aligned with the x-axis. In this principal frame of reference, the covariance matrix is diagonalized, i.e. the axes of the object will be collinear with the axes of the MagLev frame of reference. Therefore, $\mu_f^{110} = \mu_f^{101} = \mu_f^{011} = 0$ and $M_f^{110} = M_f^{101} = M_f^{011} = 0$. In this principal frame of reference, the integrals of all first order terms and second order cross-terms vanish, and the lengths of the principal axes reduces to Equations (22-24).

$$\lambda_1^2 = \frac{M_f^{200}}{M_f^{000}} = \frac{\int_{V'} x'^2 f(x',y'.z')dV'}{\int_{V'} f(x',y'.z')dV'} \tag{22}$$

$$\lambda_2^2 = \frac{M_f^{020}}{M_f^{000}} = \frac{\int_{V'} y'^2 f(x',y'.z')dV'}{\int_{V'} f(x',y'.z')dV'}. \tag{23}$$

$$\lambda_3^2 = \frac{M_f^{002}}{M_f^{000}} = \frac{\int_{V'} z'^2 f(x',y'.z')dV'}{\int_{V'} f(x',y'.z')dV'}. \tag{24}$$

2.3 Magnetic Potential Energy

We can simplify U_{mag} by applying the above steps to an object, i.e. by orienting the object in its principal frame of reference, and then by inspecting each of the nine terms separately.

$$
\begin{aligned}
U_{mag}^{200} &= \beta \sin^2\alpha \sin^2\phi \int_{V'} x'^2 \Delta\chi(\vec{r'}) dV' = \beta \sin^2\alpha \sin^2\phi M_\chi^{200} \\
&= \beta \Delta\bar{\chi} V \lambda_1^2 \sin^2\alpha \sin^2\phi \qquad (25) \\
U_{mag}^{020} &= \beta \sin^2\alpha \cos^2\phi \int_{V'} y'^2 \Delta\chi(\vec{r'}) dV' = \beta \sin^2\alpha \cos^2\phi M_\chi^{020} \\
&= \beta \Delta\bar{\chi} V \lambda_2^2 \sin^2\alpha \cos^2\phi \qquad (26) \\
U_{mag}^{002} &= \beta \cos^2\alpha \int_{V'} z'^2 \Delta\chi(\vec{r'}) dV' = \beta \sin^2\alpha M_\chi^{002} \\
&= \beta \Delta\bar{\chi} V \lambda_3^2 \cos^2\alpha \qquad (27) \\
U_{mag}^{110} &\propto \int_{V'} x'y' \Delta\chi(\vec{r'}) dV' = M_\chi^{110} = 0 \qquad (28) \\
U_{mag}^{101} &\propto \int_{V'} x'z' \Delta\chi(\vec{r'}) dV' = M_\chi^{101} = 0 \qquad (29) \\
U_{mag}^{011} &\propto \int_{V'} y'z' \Delta\chi(\vec{r'}) dV' = M_\chi^{011} = 0 \qquad (30) \\
U_{mag}^{100} &\propto \int_{V'} x' \Delta\chi(\vec{r'}) dV' = M_\chi^{100} \propto \bar{x}_\chi = 0 \qquad (31) \\
U_{mag}^{010} &\propto \int_{V'} y' \Delta\chi(\vec{r'}) dV' = M_\chi^{010} \propto \bar{y}_\chi = 0 \qquad (32) \\
U_{mag}^{001} &\propto \int_{V'} z' \Delta\chi(\vec{r'}) dV' = M_\chi^{001} \propto \bar{z}_\chi = 0 \qquad (33) \\
U_{mag}^{000} &= \beta h^2 \int_{V'} \Delta\chi(\vec{r'}) dV' = \beta h^2 \Delta\bar{\chi} V, \qquad (34)
\end{aligned}
$$

To obtain the preceding equations, we used the relations defined by equations (22), (23), and (24) along with $M_\chi^{000} = \Delta\bar{\chi}V$. The total magnetic potential energy $U_{mag} = \sum_{ijk} U_{mag}^{ijk}$ is therefore given by Equation (35).

$$
\begin{aligned}
U_{mag} &= U_{mag}^{200} + U_{mag}^{020} + U_{mag}^{002} + U_{mag}^{000} \\
&= \beta \Delta\bar{\chi} V \left(\lambda_1^2 \sin^2\alpha \sin^2\phi + \lambda_2^2 \sin^2\alpha \cos^2\phi + \lambda_3^2 \cos^2\alpha + h^2 \right) \\
&= \beta \Delta\bar{\chi} V \left[\lambda_2^2 - \lambda_3^2 + \left(\lambda_1^2 - \lambda_2^2 \right) \sin^2\phi \right] \sin^2\alpha + \beta \Delta\bar{\chi} V h^2, \qquad (35)
\end{aligned}
$$

To obtain Equation (35), we dropped terms that are constant with respect to the two degrees of freedom, α and h. We define ratios of the second moment of susceptibility R_y (Equation (36)) and R_z (Equation (37)) of the object.

$$R_y = \left(\frac{\lambda_2}{\lambda_1}\right)^2 \tag{36}$$

$$R_z = \left(\frac{\lambda_3}{\lambda_1}\right)^2, \tag{37}$$

such that

$$U_{mag} = \beta\Delta\bar{\chi}V\lambda_1^2\left[Ry - Rz + (1 - Ry)\sin^2\phi\right]\sin^2\alpha + \beta\Delta\bar{\chi}Vh^2. \tag{38}$$

This result is the full three-dimensional form of the magnetic potential energy for an arbitrary object that is parametrized within a MagLev (laboratory) frame of reference. The angle α is the angle of declination of the z'-axis from the z-axis. The angle ϕ defines the axis within the xy-plane about which the object rotates. If we did not use the principal frame of reference construction, Equations (28-33) would be non-zero and the calculations would be more complex.

2.4 Gravitational Potential Energy

Using a similar procedure, we expand the gravitational potential energy into four terms.

$$
\begin{aligned}
U_{grav}^{(100)} &= -g\sin\alpha\sin\phi\int_{V'} x'\Delta\rho(\vec{r'})dV' = -g\sin\alpha\sin\phi M_{\rho}^{100} \\
&= -mg\bar{x}'_{\rho}\sin\alpha\sin\phi \qquad (39) \\
U_{grav}^{(010)} &= g\sin\alpha\cos\phi\int_{V'} y'\Delta\rho(\vec{r'})dV' = g\sin\alpha\cos\phi M_{\rho}^{010} \\
&= mg\bar{y}'_{\rho}\sin\alpha\cos\phi \qquad (40) \\
U_{grav}^{(001)} &= g\cos\alpha\int_{V'} z'\Delta\rho(\vec{r'})dV' = g\cos\alpha M_{\rho}^{001} \\
&= mg\bar{z}'_{\rho}\cos\alpha \qquad (41) \\
U_{grav}^{(000)} &= gh\int_{V'}\Delta\rho(\vec{r'})dV' = ghM_{\rho}^{000} \\
&= mgh, \qquad (42)
\end{aligned}
$$

In this equation, $\vec{r_{\rho}}' = \left(\bar{x}'_{\rho}, \bar{y}'_{\rho}, \bar{z}'_{\rho}\right)$ is the position of the center of mass of the principal frame of reference. Equation (43) gives the total gravitational energy of the object.

$$
\begin{aligned}
U_{grav} &= mg\left(h - \bar{x}'_{\rho}\sin\alpha\sin\phi + \bar{y}'_{\rho}\sin\alpha\cos\phi + \bar{z}'_{\rho}\cos\alpha\right) \\
&= mg\left(h - \bar{r}'_{\rho}\cdot\mathbf{e}'_{z}\right), \qquad (43)
\end{aligned}
$$

In this equation, $\mathbf{e}'_{z} = e_{z}A = (\sin\alpha\sin\phi, \sin\alpha\cos\phi, \cos\alpha)$, which is the z-axis unit vector parametrized in the object frame of reference. Thus, the gravitational potential energy depends only the height of the object h and the z- component of the center of mass, as expected.

2.5 Equilibrium Height

The magnitude of the gravitational field is constant everywhere in the MagLev device, whereas the magnitude of the magnetic field depends on position. Thus, we expect the levitation height of the center of the object will not depend on the specific distribution of density within the object. It will only depend on the mean density of the object. The equilibrium height h_0 occurs where $\frac{\partial U}{\partial h} = 0$.

$$\frac{\partial U}{\partial h} = \frac{\partial U_{mag}}{\partial h} + \frac{\partial U_{grav}}{\partial h} = 2\beta\Delta\bar{\chi}Vh_0 + \Delta\bar{\rho}Vg = 0, \tag{44}$$

Equation (45) gives the equilibrium levitation height of an arbitrary object in the MagLev.

$$h_0 = -\frac{g\Delta\bar{\rho}}{2\beta\Delta\bar{\chi}}. \tag{45}$$

Expanding the constants we obtain Equation (46).

$$h_0 = \frac{(\bar{\rho}_o - \rho_m)g\mu_0 d^2}{(\bar{\chi}_o - \chi_m)4B_0^2} \tag{46}$$

This result proves that the levitation height of an object in a MagLev device (relative to the center of susceptibility of the object) *does not depend on the specific local distribution of susceptibility (and density) within the object*. The levitation height of the center of susceptibility of the object (which may differ from the centroid) is wholly determined by its mean density and mean susceptibility.

If the susceptibility (and/or the density) is distributed homogeneously (or with specific symmetries) within the object, then the center of susceptibility (and/or the center of mass) corresponds to the geometric centroid of the object. If we define h relative to the face of the bottom magnet, we obtain Equation (47).

$$h_0 = \frac{(\rho_o - \rho_m)g\mu_0 d^2}{(\chi_o - \chi_m)4B_0^2} + \frac{d}{2}, \tag{47}$$

This equation is consistent with equation 5 of Mirica *et. al.* (2).

We conclude that the position and orientation of the objects are decoupled, provided that the magnetic field is linear. Therefore, in a linear magnetic field, we can minimize with respect to the height to find the equilibrium position, and then minimize independently with respect to orientation to calculate the equilibrium orientation of an object. The decoupling allows the use of coordinate transformations such as those in Section 2.2 and 2.3 (which simplify calculations by making many terms zero), to perform calculations independent of the actual equilibrium levitation height of the object in the device.

2.6 Potential Energy of Orientation for a Homogenous Object

For objects of homogenous susceptibility and density, we can make the following simplifications: (i) $\Delta\chi(\vec{r}) = \Delta\chi$ and $\Delta\rho(\vec{r}) = \Delta\rho$; (ii) $\vec{r_\rho} = 0$ and there is no gravitational torque $\left(\frac{\partial U_{grav}}{\partial \alpha} = 0\right)$; (iii) λ_1^2, λ_2^2, and λ_3^2 reduce to the second moments of area of the object. All the objects that we tested experimentally had a pair of degenerate second moments (a square prism, a cylinder, a hollow cylinder, and an equilateral prism). The second moment of area, R_y is 1, if we orient our principal frame of reference so that the first two principal axes are degenerate ($\lambda_1 = \lambda_2$). We thus can define a single parameter, R that is a ratio of second moments that characterizes fully the behavior of objects with double degenerate geometries (Equation (48)).

$$R = \frac{Rz}{Ry} = \left(\frac{\lambda_z}{\lambda_y}\right)^2. \tag{48}$$

Equation (49) gives the total potential energy for objects with double degenerate geometries.

$$U = \beta V \Delta\chi \lambda_1^2 (Ry - Rz) \sin^2\alpha + \beta V \Delta\chi h^2 + \Delta\rho V g h. \tag{49}$$

To calculate the orientation of an object, we consider only the angle dependent part

$U(\alpha)$ of the potential energy, which is given by Equation (50).

$$\begin{aligned} U(\alpha) &= \beta V \Delta\chi \lambda_2^2 (1-R) \sin^2 \alpha \\ &\propto (1-R) \sin^2 \alpha. \end{aligned} \tag{50}$$

The equilibrium orientations occur at the local minima of $U(\alpha)$. The extrema of this function occur at $\alpha = 0$, $\pi/2$, π, and $3\pi/2$ (the function is periodic). The sign of $(1-R)$ determines which of these are minima and which are maxima. If $R < 1$, then $U(\alpha) \propto \sin^2 \alpha$ and the minima occur at $\alpha = 0$ and $\alpha = \pi$. If $R > 1$, then $U(\alpha) \propto -\sin^2 \alpha \propto \cos^2 \alpha$ and the minima occur at $\alpha = \pi/2$ and $\alpha = 3\pi/2$. If $R = 1$, then $U(\alpha) = 0$ and the potential energy is degenerate; the object does not have any preferred orientation. For this system, the orientation is completely determined by the value of R; the major axis (largest eigenvalue) of the sample will always align perpendicular to the magnetic gradient (z-axis). Intuitively, the magnetic field acts to both displace the object away from the magnets (levitation), and orient in a way such that the object appears to be "as small as possible" relative to the magnetic gradient.

2.7 The Effect of Non-Linearities of the Magnetic Field on the Orientation of Dimensionally Degenerate Objects of Homogeneous Density

We have analyzed the effects of non-linearities in the magnetic field on degenerate shapes to show that the non-linear terms qualify the energy minima. The full analysis is lengthy, thus we outline the basic steps here. First, as mentioned in the previous section, the magnetic field plateaus when approaching the surface of the magnets and has an inflexion point at the center. Therefore, the non-linearity of the field can be approximated by $\mathbf{B} = B_0 z + B_1 z^3 + O(z^5)$ where B_0 is the linear coefficient of the magnetic field and B_1 is

the cubic coefficient of the magnetic field. The contribution of the cubic term cancels part of the linear term, since the magnetic field stops increasing in magnitude as fast when away from the center.

Assuming that the higher order terms are small compared to the leading one, the magnetic energy density is then given by Equation (51).

$$u_{mag} \approx \frac{\Delta\chi}{2\mu_0} B_0^2 z^2 + \frac{\Delta\chi}{2\mu_0} 2B_0 B_1 z^4 = c_1 z^2 + c_2 z^4. \tag{51}$$

In this equation, $c_1 = \frac{\Delta\chi}{2\mu_0} B_0^2$ and $c_2 = \frac{\Delta\chi}{2\mu_0} 2B_0 B_1$ and $(c_1 > 0, |c_2| << c_1)$.

Here, $c_2 > 0$ if B_1 and B_0 have the same sign, and $c_2 < 0$ if B_1 and B_0 have different signs.

Equation (52) gives the total magnetic potential energy.

$$U_{mag} = \int_V u_{mag} = \int_{V_0} (c_1 z^2 + c_2 z^4) dV = U1 + U2, \tag{52}$$

In this equation, V_0 is the shape of the object, $U_1 = c_1 \int_{V_0} z^2 dV$, and $U_2 = c_2 \int_{V_0} z^4 dV$.

At equilibrium, this energy is again minimized as the system is conservative with no dissipation. We analyze an object oriented in its principal frame of reference and, without loss of generality, consider a 2D cross-section in the yz-plane. Since $U_1 \gg U_2$ for small objects, the behavior of a non-degenerate case ($R < 0$ or $R > 0$) is dominated by U_1, as expected, for which there are no metastable states. For the dimensionally degenerate case (R=1), such as for a square, the energy $U_1 = 0$. Within this 2D cross-section, $z = y' \sin\alpha + z' \cos\alpha$, and following a procedure similar to that in the previous section we

find that for $U_2 = \sum_{ij} U_2^{ij}$:

$$U_2^{4,0} = c_2 \sin^4 \alpha \int_{V_0} y'^4 dV \tag{53}$$

$$U_2^{3,1} = 4c_2 \cos\alpha \sin^3 \alpha \int_{V_0} y'^3 z'^1 dV \tag{54}$$

$$U_2^{2,2} = 6c_2 \cos^2 \alpha \sin^2 \alpha \int_{V_0} y'^2 z'^2 dV \tag{55}$$

$$U_2^{1,3} = 4c_2 \cos^3 \alpha \sin^1 \alpha \int_{V_0} y'^1 z'^3 dV \tag{56}$$

$$U_2^{0,4} = c_2 \cos\alpha^4 \int_{V_0} z'^4 dV, \tag{57}$$

which rely on the fourth geometric moments of the shape. For a square with side length ℓ, $U_2^{3,1} = U_2^{1,3} = 0$ the remaining potential energy is:

$$\begin{aligned} U_2 &= c_2 \frac{\ell^6}{480} \left(\cos\left(4\alpha\right) - 7\right) \\ &\propto \cos\left(4\alpha\right) \end{aligned} \tag{58}$$

For a superlinear magnetic field ($c_2 > 0$) (the field increases with an exponent greater than 1), Equation (58) shows that there are four stable configurations:
$\alpha = 0, 90°, 180°, 270°$. For a sublinear magnetic field ($c_2 < 0$), there are also four stable configurations: $\alpha = 45°, 135°, 225°, 315°$. Based on our experimental observations of the orientation of the objects, it appears that the field is slightly superlinear in our typical MagLev setup. Simulations of the magnetic field using Mathematica, also demonstrates that the field is superlinear in the vertical direction (results not shown).

3 Specific Calculations for Objects in the Experiments

In the previous sections, we demonstrated analytically how principles of symmetry in conjunction with a simplified linear form for the magnetic field provides predictions for the orientation of objects in the MagLev. Due to the minimization of magnetic potential energy, homogeneous objects can orient only along their principal axis of symmetry in a linear magnetic field. To compare theory to experiments, in this section, we present specific calculations for the objects used in our experiments. The experimental objects have a pair of degenerate principle axes ($\lambda_1 = \lambda_2$). We choose a body-fixed principal reference frame such that one of the degenerate axes (λ_1) remains collinear with the x- and x'-axes. In this reference frame, all rotation is constrained to the yz-plane (around the x- and x'-axes). We can, therefore, use Equation (50) to analyze the change in potential energy due to the orientation of the object. We define a unit vector $\mathbf{p}$ perpendicular to the face that spans the degenerate principal axes, and measure the angle α as the angle of inclination between $\mathbf{p}$ and the $z-$axis (Fig. 2 in the main paper and Fig. S8). We prepare the object in an initial state $\alpha = 0$ (configuration 1). We expect that an object will abruptly transition from $\alpha = 0$ to $\alpha = 90\,^\circ$ (configuration 2) when its second moment ratio R transitions from $R < 1$ to $R > 1$. R can be calculated using Equation (59).

$$R = \left(\frac{\lambda_3}{\lambda_2}\right)^2 = \frac{\int_V z^2 dV}{\int_V y^2 dV} \tag{59}$$

Although R is a parameter that wholly predicts the orientation of a homogeneous object in a linear field, this value cannot, typically, be easily measured experimentally. We parametrize our objects with a pair of length parameters, ℓ for the characteristic width of the face of the object, and T for the thickness (Fig. S8). Here we calculate R for various shapes and relate it to the the easily measured aspect ratio, $A_R = T/\ell$. In the experiments,

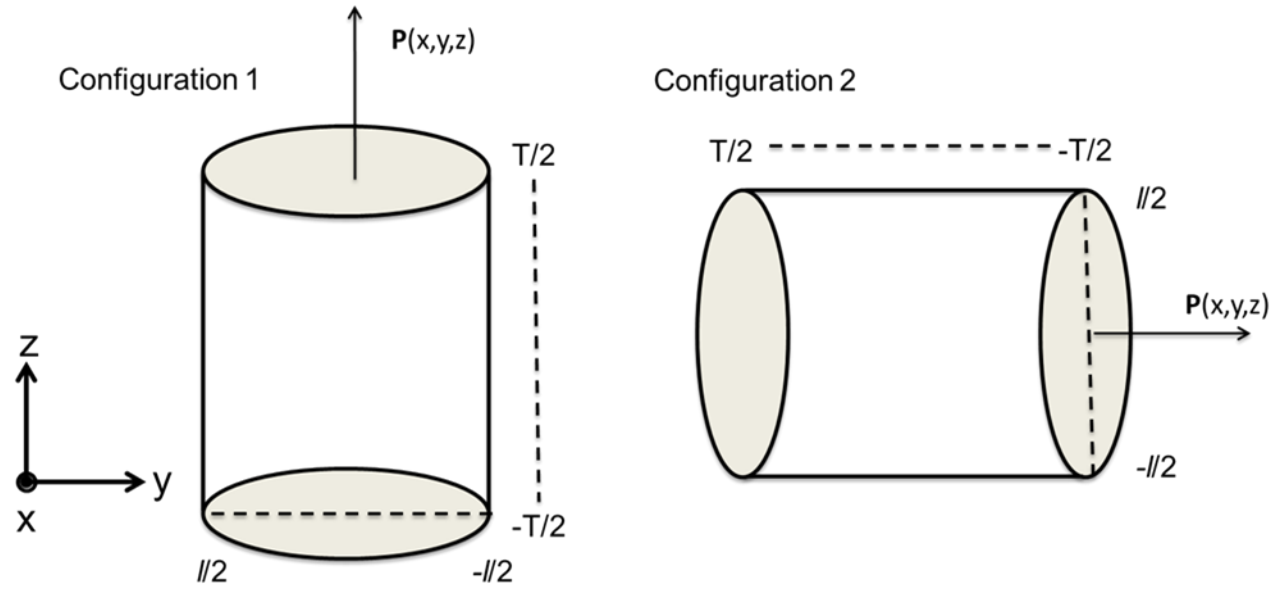

Figure S8: Sketch of the configuration of a cylinder with the bounds of integration marked.

one dimension (ℓ) was kept constant while the other (T) was varied so as to change A_R (and therefore R).

3.1 Solid block of cross section area $\ell \times \ell$ and length T

For a solid rectangular block, we use Cartesian coordinates for integration.

$$R = \frac{\int_{V_0} z^2 dV}{\int_{V_0} y^2 dV} = \frac{\int_{-T/2}^{T/2} z^2 dz \int_{-\ell/2}^{\ell/2} dy \int_{-\ell/2}^{\ell/2} dx}{\int_{-T/2}^{T/2} dz \int_{-\ell/2}^{\ell/2} y^2 dy \int_{-\ell/2}^{\ell/2} dx} = \frac{l^2 T^3/12}{\ell^4 T/12} = \frac{T^2}{\ell^2} = A_R^2, \tag{60}$$

and therefore

$$A_R = \sqrt{R}. \tag{61}$$

The critical aspect ratio is therefore $A_R = 1$, matching experiment. For $A_R < 1$, the object will orient in configuration 1.

3.2 Solid cylinder of diameter ℓ and height T

For a solid cylinder, we use cylindrical coordinates to simplify integration.

$$R = \frac{\int_{V_0} z^2 dV}{\int_{V_0} y^2 dV} = \frac{\int_{-T/2}^{T/2} z^2 dz \int_0^{2\pi} d\phi \int_0^{\ell/2} r dr}{\int_{-T/2}^{T/2} dz \int_0^{2\pi} \int_0^{\ell/2} (r\sin\phi)^2 r dr d\phi} = \frac{\frac{\pi}{48}\ell^2 T^3}{\frac{\pi}{64}\ell^4 T} = \frac{4T^2}{3\ell^2} = \frac{4}{3}A_R^2, \tag{62}$$

and therefore

$$A_R = \sqrt{\frac{3}{4}R}. \tag{63}$$

The critical aspect ratio is therefore $A_R = \sqrt{3/4} \approx 0.86$, matching experiment. For $A_R < 0.86$, the object will orient in configuration 1.

3.3 Hollow cylinder of outer diameter ℓ, inner diameter $\epsilon\ell$ and length T

.

For a hollow cylinder, we continue use cylindrical coordinates to simplify integration.

$$R = \frac{\int_{V_0} z^2 dV}{\int_{V_0} y^2 dV} = \frac{\int_{-T/2}^{T/2} z^2 dz \int_0^{2\pi} d\phi \int_{\epsilon\ell/2}^{\ell/2} r dr}{\int_{-T/2}^{T/2} dz \int_0^{2\pi} \int_{\epsilon\ell/2}^{\ell/2} (r\sin\phi)^2 r dr d\phi} = \frac{\frac{\pi}{48}\ell^2 T^3(1-\epsilon^2)}{\frac{\pi}{64}\ell^4 T(1-\epsilon^4)} \tag{64}$$

$$= \frac{4(1-\epsilon^2)T^2}{3(1-\epsilon^4)\ell^2} = \frac{4(1-\epsilon^2)}{3(1-\epsilon^4)}A_R^2, \tag{65}$$

and therefore

$$A_R = \sqrt{\frac{3}{4}\frac{(1-\epsilon^4)}{(1-\epsilon^2)}R}. \tag{66}$$

We note that increasing ϵ (making a hollow cylinder) will increase the critical aspect ratio for the change in orientation - indeed we get critical aspect ratios that are greater than unity for a range of ϵ. When $\epsilon = 0$, we recover the result for a solid cylinder. When $\epsilon = 1$, there is no cylinder. For a range of ϵ, we have critical aspect ratios of greater than unity. For the experiments the outer diameter of the hollow cylinder is 1/4 inch and the thickness

of the wall is 1/32 inch (i.e. $\epsilon = 3/4$). Substituting these values, we find the critical aspect ratio to be $A_R \approx 1.09$ matching experiment. For $A_R < 1.09$, the object will orient in configuration 1.

3.4 Triangular block

For a triangular block, we use Cartesian coordinates to parametrize the limits of integration.

$$R = \frac{\int_{V_0} z^2 dV}{\int_{V_0} y^2 dV} = \frac{\int_{-T/2}^{T/2} z^2 dz \int_{-l/2}^{l/2} dx \int_{-\ell/2\sqrt{3}}^{-\sqrt{3}|x|+\ell/\sqrt{3}} dy}{\int_{-T/2}^{T/2} dz \int_{-l/2}^{l/2} dx \int_{-\ell/2\sqrt{3}}^{-\sqrt{3}|x|+\ell/\sqrt{3}} y^2 dy} = \frac{\frac{1}{16\sqrt{3}}\ell^2 T^3}{\frac{1}{32\sqrt{3}}\ell^4 T} \tag{67}$$

$$= 2\frac{T^2}{\ell^2} = 2A_R^2, \tag{68}$$

and therefore

$$A_R = \sqrt{\frac{R}{2}}. \tag{69}$$

The critical aspect ratio is therefore $A_R = \sqrt{1/2} \approx 0.70$, matching experiment. For $A_R < 0.7$, the object will orient in configuration 1.

Supporting Information References

1. Jackson JD (1998) *Classical Electrodynamics* (John Wiley Sons, New York) 3 Ed.

2. Mirica KA, Shevkoplyas SS, Phillips ST, Gupta M, Whitesides GM (2009) Measuring densities of solids and liquids using magnetic levitation: Fundamentals. *J. Am. Chem. Soc.* 131(29):10049-10058.